The Journal of Immunology

# High-Fat Diet Rapidly Modifies Trafficking, Phenotype, and Function of Plasmacytoid Dendritic Cells in Adipose Tissue

Susanne Stutte, Hellen Ishikawa-Ankerhold, Lydia Lynch, Sarah Eickhoff, Simona Nasiscionyte, Chenglong Guo, Dominic van den Heuvel, Daniel Setzensack, Marco Colonna, Daniela Maier-Begandt, Ludwig Weckbach, Thomas Brocker, Christian Schulz, Barbara Walzog and Ulrich von Andrian

*J Immunol* 2022; 208:1445-1455; Prepublished online 18 February 2022;
doi: 10.4049/jimmunol.2100022
http://www.jimmunol.org/content/208/6/1445



*The Journal of Immunology* is published twice each month by
The American Association of Immunologists, Inc.,
1451 Rockville Pike, Suite 650, Rockville, MD 20852

Print ISSN: 0022-1767 Online ISSN: 1550-6606.

# High-Fat Diet Rapidly Modifies Trafficking, Phenotype, and Function of Plasmacytoid Dendritic Cells in Adipose Tissue

**Susanne Stutte,[*,†,‡,§] Hellen Ishikawa-Ankerhold,[†,¶] Lydia Lynch,[§,‖] Sarah Eickhoff,[#,1] Simona Nasiscionyte,[†] Chenglong Guo,[†,¶] Dominic van den Heuvel,[†,¶] Daniel Setzensack,[†,¶] Marco Colonna,[**] Daniela Maier-Begandt,[*,†] Ludwig Weckbach,[*,†,¶] Thomas Brocker,[‡] Christian Schulz,[†,¶] Barbara Walzog,[*,†] and Ulrich von Andrian[§,††]**

**Plasmacytoid dendritic cells (pDCs) display an increased abundance in visceral adipose tissue (VAT) of humans with obesity. In the current study, we set out to decipher the molecular mechanisms of their recruitment to VAT and the functional relevance of this process. We observed increased pDC numbers in murine blood, liver, spleen, and VAT after feeding a high-fat diet (HFD) for 3 wk when compared with a standard diet. pDCs were enriched in fat-associated lymphoid clusters representing highly specific lymphoid regions within VAT. HFD led to an enlargement of fat-associated lymphoid clusters with an increased density and migratory speed of pDCs as shown by intravital multiphoton microscopy. For their recruitment into VAT, pDCs employed P-selectin with E-selectin and L-selectin being only critical in response to HFD, indicating that the molecular cues underlying pDC trafficking were dependent on the nutritional state. Subsequent recruitment steps required $\alpha_4\beta_1$ and $\alpha_4\beta_7$ integrins and engagement of CCR7. Application of fingolimod (FTY720) abrogated egress of pDCs from VAT, indicating the involvement of sphingosine-1-phosphate in this process. Furthermore, HFD altered pDC functions by promoting their activation and type 1 IFN expression. Blocking pDC infiltration into VAT prevented weight gain and improved glucose tolerance during HFD. In summary, a HFD fundamentally alters pDC biology by promoting their trafficking, retention, and activation in VAT, which in turn seems to regulate metabolism.** ***The Journal of Immunology*****, 2022, 208: 1445–1455.**

Obesity is a major risk factor for metabolic diseases and became an enormous health burden in modern societies in the last 30 years (1). Excessive nutritional energy is stored in the white adipose tissue dispersed s.c. throughout the body and between internal organs. It serves as a major lipid reservoir and additionally as a source of endocrine mediators. Especially, visceral adipose tissue (VAT) is recognized to be highly metabolic active in humans (2). In mice, white adipose tissue attached to the uterus of females or epididymis of males is primarily known as VAT. In recent years it has become evident that excessive nutritional intake does not only affect body weight and disturb metabolism, but it also dramatically influences immunological homeostasis (3, 4). In VAT, classical dendritic cells (DCs) (5), invariant NK T cells (6), and γδ T cells (7) decrease with obesity whereas $CD8^+$ T cells (8), innate lymphoid cells (9), and macrophages change in composition and performance. VAT-resident immune cells have a variety of different functions, including the regulation of adipokine expression, clearance of apoptotic cells, and extracellular matrix remodeling (3, 10). The shift of immune cell composition, numbers, and phenotype initiated with obesity finally results in a switch toward a proinflammatory cytokine milieu (11–13) that leads to a systemic increase of different inflammatory mediators, including free fatty acids, TNF-α, IL-1β, and IL-6 (14, 15), which in turn promote the development of insulin insensitivity and metabolic diseases (16).

*Institute of Cardiovascular Physiology and Pathophysiology, Biomedical Center, Ludwig-Maximilians-Universität München, Planegg-Martinsried, Germany; †Walter Brendel Center of Experimental Medicine, University Hospital, Ludwig-Maximilians-Universität München, Munich, Germany; ‡Institute for Immunology, Faculty of Medicine, Ludwig-Maximilians-Universität München, Munich, Germany; §Department of Immunology, Blavatnik Institute, Harvard Medical School, Boston, MA; ¶Department of Internal Medicine I, University Hospital, Ludwig-Maximilians-Universität München, Munich, Germany; ‖Trinity Biomedical Science Institute, Trinity College Dublin, Dublin, Ireland; #Institute of Systems Immunology, University of Würzburg, Würzburg, Germany; **Washington University, School of Medicine, St. Louis, MO; and ††Ragon Institute of MGH, MIT and Harvard, Cambridge, MA

[1]Current address: Institute of Experimental Oncology, University of Bonn, Bonn, Germany.

ORCIDs: 0000-0003-0277-6403 (S.S.); 0000-0003-0307-7022 (H.I.-A.); 0000-0003-1327-7351 (S.E.); 0000-0002-8998-0396 (D.v.d.H.); 0000-0002-5026-3242 (D.S.); 0000-0001-7060-5433 (T.B.); 0000-0002-8149-0747 (C.S.); 0000-0001-7729-6565 (B.W.); 0000-0003-4231-2283 (U.v.A.).

Received for publication January 11, 2021. Accepted for publication January 5, 2022.

This work was supported by Deutsche Forschungsgemeinschaft Grants STU 528/1-1 (to S.S.), SFB 1054 B03 (to T.B.), SFB 914 A06 (to S.S. and T.B.), SFB 914 A02 (to B.W. and D.M.-B.), SFB 914 B10 (to L.W.), SFB 914 Z01 (to H.I.-A.), and SFB 914 A10 (to C.S.), Friedrich Baur-Stiftung (to S.S.), and by National Institute of Allergy and Infectious Diseases Grant R01 AI155865 (to U.v.A.).

S.S. designed the study, analyzed the data, and wrote the paper. S.S., H.I.-A., S.N., C.G., D.v.d.H., D.S., L.L., and S.E. performed experiments. T.B., M.C., and C.S. provided reagents and mice; L.W. provided reagents, and D.M.-B. and B.W. contributed in paper writing and provided reagents. U.v.A. designed the study, provided reagents and mice, and was involved in writing the paper. All authors discussed the results and commented on the manuscript.

Address correspondence and reprint requests to Dr. Susanne Stutte, Institute of Cardiovascular Physiology and Pathophysiology, Biomedical Center, Ludwig-Maximilians-Universität München, Großhaderner Strasse 9, 82152 Planegg-Martinsried, Germany. E-mail address: susanne.stutte@med.uni-muenchen.de

The online version of this article contains supplemental material.

Abbreviations used in this article: BM, bone marrow; DC, dendritic cell; FALC, fat-associated lymphoid cluster; FTY720, fingolimod; GPCR, G protein–coupled receptor; HEV, high endothelial venule; HFD, high-fat diet; IFN-I, type I IFN; IPGTT, i.p. glucose tolerance test; LN, lymph node; MFI, mean fluorescence intensity; MOB, messenger of IFN-β; pDC, plasmacytoid DC; PTx, pertussis toxin; SFD, standard fat diet; SiglecH, sialic acid binding Ig-like lectin H; S1P, sphingosine-1-phosphate; S1PR, S1P receptor; VAT, visceral adipose tissue; WT, wild-type.

Within the white adipose tissue, clusters of hematopoietic cells have been identified and named fat-associated lymphoid clusters (FALCs) (17). These non-classical lymphoid clusters have been described in omental, mesenteric, gonadal, and pericardial fat (17, 18). Composed of B1 and B2 cells (19), $CD4^+$ T cells, and $CD11b^+$ myeloid cells (18), FALCs are highly vascularized (18) and, in contrast to lymph nodes (LNs), they are not encapsulated (17). However, FALCs of the omentum contain high endothelial venules (HEVs) (20), a specialized type of postcapillary venule essential for lymphocyte trafficking to LNs. Interestingly, FALCs increase in number and size in response to acute or chronic inflammation of the peritoneal cavity to initiate adaptive immune responses (17, 18, 21).

Recently, plasmacytoid DCs (pDCs) gained attention, as these rare innate immune cells increase in frequency in VAT and liver of obese mice and humans (22–24). In contrast to classical DCs, pDCs have a round morphology and are characterized by their secretory function (25). They are capable to sense viruses and self-nucleic acids (26) and respond with rapid and robust type 1 IFN (IFN-I) expression and secretion (27). Despite few molecular differences, the function, the overall phenotype, and the core gene expression program is conserved between human and murine pDCs (28), and several pDC-specific surface markers have been established. Murine pDCs express sialic acid binding Ig-like lectin H (SiglecH), plasmacytoid dendritic cell Ag-1 (PDCA-1, CD317), Ly6C, and CD45R. In steady state, pDCs express low levels of MHC class II and costimulatory molecules and their expression increases upon activation (29). The generation of pDCs is mainly restricted to the bone marrow (BM), from where they enter the blood and secondary lymphoid organs to continuously patrol through the body. In the LN, they reach T cell areas mainly through HEVs by employing a specific adhesion cascade (30, 31). Under steady-state conditions, pDCs require L-selectin and during inflammation additionally E-selectin to allow rolling in the LN (32). Furthermore, $\beta_1$ and $\beta_2$ integrins as well as multiple chemokine receptors such as CCR7 and CCR9 are essential for pDCs to adhere and transmigrate into the LN, gut, and thymus tissue (33, 34). Similar to T cells, pDCs egress from secondary lymphoid organs back into the blood by sphingosine-1-phosphate (S1P)–mediated signaling (35). S1P is a lipid mediator that is present at high concentrations in plasma and lymph and couples to five different G protein–coupled S1P receptors (S1PRs) (36). The decisive role of S1P in immune cell trafficking was discovered when the immunosuppressive agent fingolimod (FTY720) was found to induce S1PR1, S1PR3, S1PR4, and S1PR5 internalization in T cells to render them unresponsive to the S1P gradient toward the circulation trapping them in secondary lymphatic organs (37, 38).

Within the immune system, pDCs are key players in orchestrating sensitization, activation, and differentiation of innate and adaptive immune cells (39). Interestingly, gene expression analyses during obesity show an upregulation of IFN-I genes in VAT (40), and IFN-I receptor-deficient mice fail to develop obesity and insulin insensitivity (24). Furthermore, recent studies suggest that pDCs, which represent a major source of IFN-I, may play a critical role in promoting obesity (41). In this study, we set out to decipher the impact of a high-fat diet (HFD) on the trafficking of pDCs into VAT and their activation within this key region of obesity. We identified the localization of pDCs in VAT and their multistep adhesion cascade facilitating their homing into VAT. HFD resulted not only in increased pDC infiltration and retention, but it also promoted an activated pDC phenotype compared with a standard fat diet (SFD). Within VAT, pDCs accumulated in FALCs where they increased in density and mobility after HFD application. The blockade of pDC infiltration to adipose tissue prevented weight gain and improved glucose tolerance. In summary, we identified a unique trafficking and activation profile of pDCs within VAT in response to HFD that opens up new avenues for treatment of obesity by targeting pDC homing and activation.

## Materials and Methods

### *Animals*

C57BL/6 wild-type (WT) mice were purchased from Charles River Laboratories (Wilmington, MA). $CCR7^{-/-}$ mice were bred and housed in the animal facilities of the New Research Building, Harvard Medical School (Boston, MA). The ubiquitin C–tdTomato mice provided by Wolfgang Kastenmüller (MPI Würzburg, Würzburg, Germany) and the SiglecH-GFP reporter mice (42) were bred in the animal facility of the University of Bonn (Bonn, Germany). Homozygous messenger of IFN-β (MOB) mice were obtained from Stefanie Scheu (HHU Düsseldorf, Düsseldorf, Germany) (43). Mice were housed under specific pathogen–free conditions in accordance with National Institutes of Health guidelines. Animal experiments have been approved by the Institutional Review Board and local authorities. Experiments were performed with mice at 6–10 wk of age at Harvard Medical School (Boston, MA), the University of Bonn, the Biomedical Center of the Ludwig-Maximilians-Universität München, and at the Multiphoton Imaging Core Facility at the Walter Brendel Center of Experimental Medicine in Munich, Germany. Normal chow, HFD (Research Diets, open source; D12492), or SFD (Research Diets, open source; D12450J) were applied for 3 wk.

### *Ab staining and flow cytometry*

Unless stated otherwise, all Abs were obtained from BioLegend. The following anti-mouse Abs were used: CD31 (390), SiglecH (551-PE or -FITC), CD45R (RA3-6B2), CD11b (M1/70), CD45 (30-F11), PDCA-1 (927), CD49d (R1-2), CD62L (MEL-14), CXCR3 (CXCR3-176), and CCR7 (4B12). E-selectin and P-selectin binding sites on pDCs were evaluated by staining with E-selectin–human Ig Fc chimera (R&D Systems) and P-selectin–human Ig Fc chimera Ab (R&D Systems). Staining for flow cytometry was performed at 4°C for 20–30 min in FACS buffer (1% FCS in PBS with 2 mM EDTA). Dead cells were excluded by staining with Zombie Aqua (BioLegend, 1:1000 in PBS). Data were acquired by using FACSCanto II (Becton Dickinson) and analyzed with FlowJo software (Becton Dickinson). For in vivo imaging, SiglecH-Alexa 488, CD45-PE, and CD31-Alexa 647 were used.

### *Statistical analysis*

All data are presented as mean ± SEM. Significance was calculated with GraphPad Prism 8. Statistical analyses were performed using a Student *t* test or one-way ANOVA as indicated. Significance was defined as follows: $*p < 0.05$, $**p < 0.01$, $***p < 0.001$, and $****p < 0.0001$.

### *In vivo and in vitro expansion of pDCs*

Female C57BL/6 mice were injected s.c. with melanoma cell line B16 secreting FLT3L that results in a massive expansion of all DC subsets in vivo (4, 44). Seven days after inoculation, spleen and liver were harvested and pDCs were enriched by gradient centrifugation (Lymphoprep, STEMCELL Technologies) at 800 × *g* for 20 min at 20°C without a break. pDC content and number were measured by flow cytometry staining before transfer. Cell suspensions were stained with CSFE (Molecular Probes). When indicated, pDCs were generated in vitro by incubating BM with FLT3L for 7 d. Cells were harvested and pDCs were quantified by FACS staining before labeling with a CellTrace Violet cell proliferation kit (Invitrogen).

### *Pertussis toxin pretreatment*

pDCs were treated with pertussis toxin (PTx) (final concentration 200 ng/ml) for 2 h at 37°C and combined with CSFE labeling during the last 20 min before washing with RPMI 1640 containing 2% FCS. Media-treated pDCs were mixed with differentially stained cells and injected (in 200 μl of solution) into the tail veins of mice.

### *Homing assays*

Enriched labeled pDCs were suspended in 2–4 × $10^7$ cells/ml and injected i.v. After 18 h, recipient mice were sacrificed and spleen, inguinal LNs, liver, and VAT were harvested and analyzed by flow cytometry. Homing of pDCs was calculated to the number of injected pDCs. For inhibitory studies, the number of transferred pDCs was measured and pDCs recovered 18 h later in different organs were calculated per 1 million injected pDCs. In competitive homing assays, WT and $CCR7^{-/-}$ cells were either stained with CFSE or with tetramethylrhodamine-5-isothiocyanate (TRITC; Molecular Probes). Switching labeling ensured no effect of toxicities for either cell population.

An index for homing was calculated by a ratio of PTx-treated or CCR7$^{-/-}$ versus control cells (100%).

### *Blocking Abs for inhibition studies*

The following mAbs were used: Mel-14 (rat IgG2a, anti-murine L-selectin (45), Bio X Cell] and PS/2 (rat IgG2b, anti-murine α4), which were stored at −70°C in endotoxin-free saline at 1 mg/ml. P-selectin and E-selectin were blocked with RMP-1 and ultra-RME-1/CD62E (BioLegend), respectively. The integrin $\alpha_4\beta_7$ (LPAM) was blocked with DATK32 (BioLegend), CCR9 with blocking Abs (9B1, BioLegend), and CXCR3 with blocking Abs (CXCR3-173, BioLegend). For inhibition studies, 100 μg of Ab was directly injected i.v. before cell transfer (~1–2 h) or coinjected with pDC suspension. Administration of the S1PR inhibitor FTY720 (1 mg/kg) or PBS was performed as indicated or by daily i.p. injections.

For long-term blockade mice were fed with SFD (D12450J, Research Diets) or HFD (D12492, Research Diets) for 1 wk and injected daily i.p. with 100 μg of mAb against P-selectin (BioLegend) or its isotype control (IgG2a, MOPC-173). Mice were weighed daily and the weight of VAT was analyzed on day 7. Glucose tolerance was tested (i.p. glucose tolerance test [IPGTT]) by injecting 1 mg/kg glucose (Life Technologies) i.p. into 5-h-starved mice. The level of blood glucose was measured at 10-min intervals until 90 min after glucose injection.

### *Tissue preparation*

LN, spleen, liver, and epididymal VAT were harvested 18 h after pDC transfer. LNs were smashed through a nylon net (pore size 70 μm). Spleen was digested with collagenase D (1 mg/ml) and DNase 1 (1 mg/ml) for 20 min at 37°C in RPMI 1640 media. Subsequently, the tissue was smashed through a nylon net and RBC lysis (Pharm Lyse, BD Biosciences) was performed before FACS staining. Liver was smashed through a nylon net by scraping it with a lid of the petri dish with PBS and 2 mM EDTA. The cell suspension was placed on a Lymphoprep gradient (STEMCELL Technologies) and centrifuged at 800 × *g* without break for 20 min at room temperature. Cells were harvested from the interphase, washed with PBS, and stained with Abs for flow cytometry. VAT tissue was minced with a scalpel and digested with collagenase 2 (1 mg/ml in RPMI 1640 media) for 25 min at 37°C under continuous rotation. The suspension was centrifuged and the cell pellet (stromal-vascular fraction) was taken up in RBC lysis buffer before staining for flow cytometry.

For the ELISA of IFN-α (PBL IFN Source) and IFN-β (BioLegend) one fat pad of epididymal VAT was lysed in T-PER tissue protein extraction reagent (Thermo Fisher Scientific) with protease inhibitor (Roche). The amount of cytokine was calculated per one total fat pad.

### *Intravital multiphoton imaging*

In female mice VAT is directly attached to the uterus. When establishing the imaging protocol, we observed that the uterus contracted uncontrollably, which led to unwanted movements in the videos. Therefore, we preferred male mice for in vivo imaging. C57BL/6 mice were anesthetized with an i.p injection of MMF-mix anesthesia (5.0 mg/kg midazolam, 0.5 mg/kg medetomidine, and 0.05 mg/kg fentanyl). SiglecH-FITC and CD45-PE Abs were injected i.v. 15 min before imaging. When indicated, isolated SiglecH-GFP cells from BM and liver of SiglecH GFP reporter mice (46) were injected i.p. 6 or 12 h before imaging the rear side of the VAT (facing the intestine).

pDCs from SiglecH-GFP reporter mice were enriched from bone marrow and transferred via i.p. injection into ubiquitin C−tdTomato mice. Eighteen hours later, mice were anesthetized with isoflurane (Baxter; 2.5% for induction, 1–1.5% for maintenance, vaporized in an 80:20 mixture of $O_2$ and air), VAT was exposed, and intravital microscopy was performed. The imaging system was composed of a Zeiss 780 upright microscope equipped with a 20-water immersion lens (numerical aperture 1.0; Zeiss), a Chameleon laser (Coherent) tuned to 820 or 930 nm, and with the ZEN acquisition control software. The microscope was enclosed in an environmental chamber in which anesthetized mice were warmed by heated air and the VAT was kept at 37°C with warmed PBS. Raw imaging data were processed and analyzed with Imaris (Bitplane). In addition, imaging was performed using a LaVision BioTec multiphoton TriM Scope II equipped with a Chameleon pulsed laser with the range from 800 to 1100 nm. The images were acquired by Inspector software and processed with Imaris (Bitplane).

### *Confocal imaging of VAT*

VAT was harvested and fixed using PLP buffer (0.05 M phosphate buffer containing 0.1 M L-lysine [pH 7.4], 2 mg/ml $NaIO_4$, and 10 mg/ml paraformaldehyde) for 6 h, then dehydrated in 30% sucrose and stained. Tissue was permeabilized, blocked, and stained in PBS containing 0.3% Triton X-100 and 1% FCS in a humidified chamber (overnight, 4°C). After washing, the tissue was mounted with GenTeal gel (Novartis) or Dako and imaged as whole mount with the Olympus FluoView BX50WI inverted microscope with 10×/0.4 and 20×/0.5 objectives or with an LSM 880 with Airyscan module (Carl Zeiss), with EC Plan-Neofluar 10×/0.3 and Plan-Apochromat 20×/0.8 objectives. Image analysis was performed using ImageJ software (National Institutes of Health) or with Zen blue software (Carl Zeiss).

### *Real-time PCR*

Liver, spleen, LNs, and VAT were placed in TRIzol (Ambion) and minced. RNA extraction was performed with a Qiagen RNeasy kit, and cDNA synthesis was performed with an iScript kit (Bio-Rad). RT-PCR was performed on a LightCycler 480 II (Roche) using a SYBR Green QuantiFast kit (Qiagen). Relative gene expression was calculated using the ΔCt method, and the mean expression level of liver from SFD was set as 1. The following primers were designed with Roche probe library: CCL19 forward, 5′-TGTGGC CTGCCTCAGATTAT-3′, reverse, 5′-AGTCTTCCGCATCATTAGCAC-3′; CCL21a forward, 5′-TCCAAGGGCTGCAAGAGA-3′, reverse, 5′-TGAAGTTCGTGGGGGATCT-3′; CCL21b forward, 5′-TCCAAGGGCTG CAAGAGA-3′, reverse, 5′-TGAAGTTCGTGGGGGATCT-3′; CCL25 forward, 5′-GAGTGCCACCCTAGGTCATC-3′, reverse, 5′-CCAGCTGGT GCTTACTCTGA-3′; CD62E (sele) forward, 5′-TCCTCTGGAGAGTG GAGTGC-3′, reverse, 5′-GGTGGGTCAAAGCTTCACAT-3′; CD62P (selp) forward, 5′-TCCAGGAAGCTCTGACGTACTTG-3′, reverse, GCAGCG TTAGTGAAGACTCCGTAT-3′; as the housekeeping gene, 18S rRNA was used, forward, 5′-GCCGCTAGAGGTGAAATTCTT-3′, reverse, 5′-CGTCT TCGAACCTCCGACT-3′.

## Results

### *HFD induces systemic increase of pDCs*

In humans, pDC numbers in VAT correlate with an increase in body mass index (24), suggesting that obesity may affect the homeostasis of pDCs. Therefore, we studied whether high fat intake alone was instrumental in provoking systemic alterations of the pDC profile within the body. We fed male mice for 3 wk with either HFD or SFD as control, and subsequently analyzed blood, peripheral tissue, lymphatic organs, and VAT for the presence of pDCs by flow cytometry (Supplemental Fig. 1A, 1B). The HFD mediated a gain in body weight (Fig. 1A) and increased pDC numbers in blood and tissues (Fig. 1B, Supplemental Fig. 1C–E). In LNs, the absolute pDC number was reduced, which coincided with a decreased total number of CD45$^+$ cells in the LNs with a HFD (data not shown and Ref. 47). However, the pDC frequency in the LN revealed no change. The VAT increased 2-fold in weight after 3 wk of a HFD, and it displayed increased pDC numbers and frequency (Fig. 1C, Supplemental Fig. 1C–E). Thus, application of HFD altered pDC homeostasis throughout the body. This observation was largely independent of sex, as female mice presented a similar systemic increase in pDC number with a HFD with the exception of BM (Supplemental Fig. 2A–C). Thus, an obesogenic diet for only 3 wk fundamentally modified the presence of pDCs in VAT.

### *pDC localization in FALCs*

Next, we studied the distribution profile of pDCs in VAT and found that they were present in CD45$^+$ cell clusters (defined as accumulation of more than five CD45$^+$ cells, minimal diameter of 50 μm, and minimal proximity between cells of 10 μm), so-called FALCs, which mainly localized in the peripheral area of the tip part of the epididymal VAT (Fig. 2A, 2B, blue areas). In 3-wk-old mice, only some VAT-pDCs were detectable at CD31$^+$ blood vessels and FALCs were absent (Fig. 2C, left), whereas 8-wk-old mice presented FALCs (Fig. 2C, right), suggesting that FALCs develop in postnatal life. When mice were fed with HFD for 3 wk, FALCs significantly increased in number from ~22 to 38 per mm$^3$ (Fig. 2D, 2E). A 3-fold increased mean fluorescence intensity (MFI) of CD45 within the FALCs after feeding a HFD further indicated an accumulation of CD45$^+$ cells in VAT resulting in a larger size of FALCs (Fig. 2D, 2F). Thus, a HFD promotes FALC formation and enlargement. Next, we established intravital multiphoton microscopy to

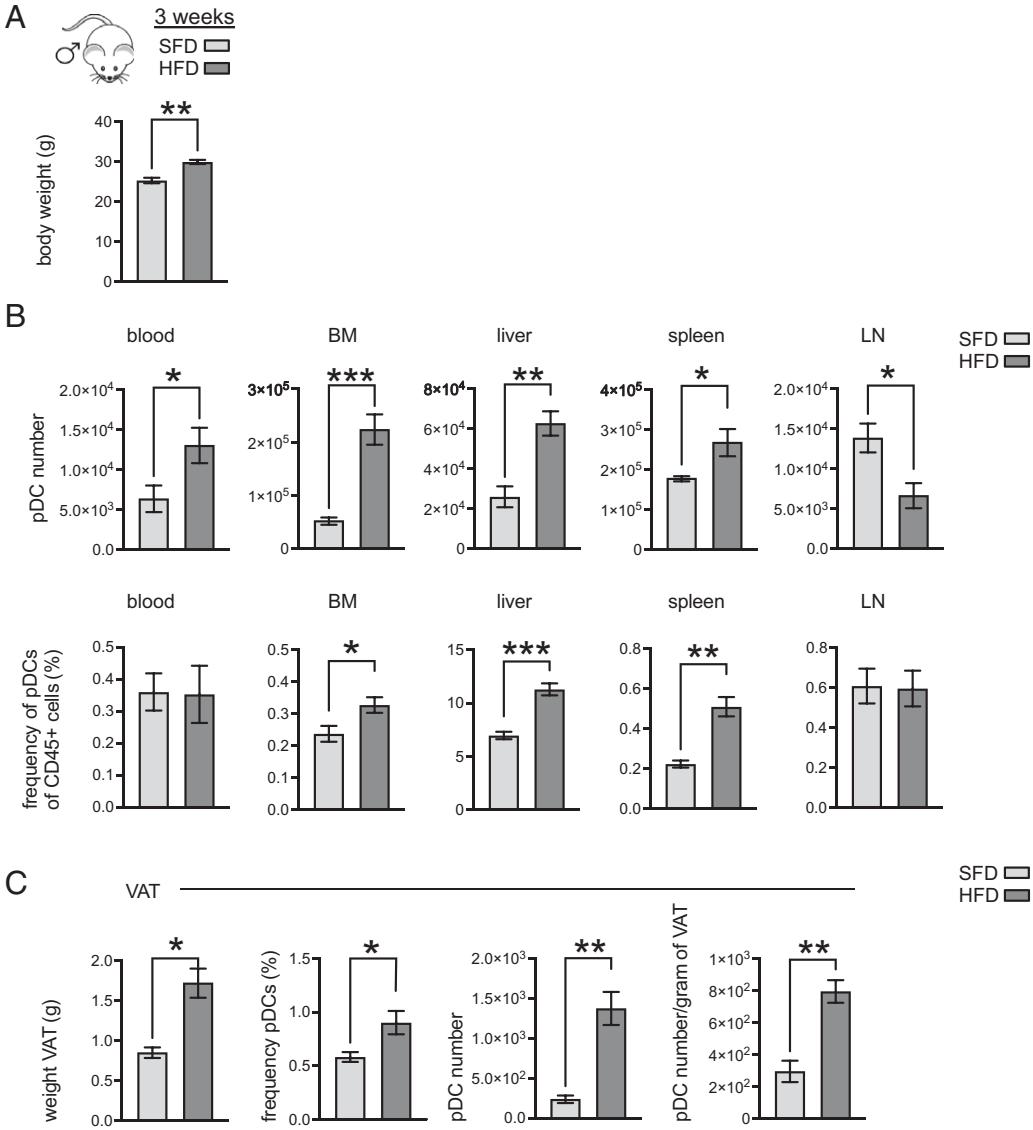


**FIGURE 1.** HFD induced a systemic increase of pDCs. (**A**) C57BL/6 male mice were fed for 3 wk a standard fat diet (SFD, gray, D12450J) or high-fat diet (HFD, dark gray, D12492) and body weight was measured at day of analysis. (**B**) Blood and single-cell suspensions of different peripheral and lymphoid tissues of mice were analyzed by flow cytometry. Absolute pDC numbers were calculated per 1 ml of blood or per total organ or per one femur, and pDC frequency was calculated as percentage of $CD45^+$ cells (100%). BM, bone marrow; LN, inguinal lymph node. (**C**) Weight of visceral adipose tissue (VAT) was measured and pDC frequency of $CD45^+$ and number was determined. pDC numbers per 1 g of VAT were calculated. For (A)–(C), the animal experiment was repeated three times with four animals per group and similar outcome. One representative experiment is shown. Statistical analyses were performed using a Student *t* test. Values represent mean ± SEM. $*p < 0.05$, $**p < 0.01$, $***p < 0.001$.

uncover the mobility of pDCs in VAT in detail. Isolated SiglecH-$GFP^+$ pDCs were transferred into mice ubiquitously expressing tdTomato to identify the tissue structure, including hematopoietic cells, blood vessels, stromal cells, and adipocytes. After 18 h, pDCs were found in peripheral areas of VAT (Supplemental Fig. 2D). Interestingly, most pDCs were present within clusters of $tdTomato^+$ cells (Supplemental Fig. 2D, Supplemental Video 1). Again, these clusters were localized in the tip area, similar to the $CD45^+$ clusters, the so-called FALCs, indicating the dynamics of pDC trafficking into FALCs (see Fig. 2A). Intravital imaging confirmed that the increase of FALCs upon HFD (Fig. 2G) was accompanied by a substantial rise in VAT-resident pDCs (Fig. 2H, left), which preferentially localized within the FALCs. In this study, the abundance of pDCs in the FALCs increased from ~18 cells per $mm^2$ with SFD to 63 cells per $mm^2$ with HFD (Fig. 2H, middle). The migratory speed of endogenous pDCs in VAT changed from resident-like (3 μm/min) to migratory (10 μm/min) behavior (Fig. 2H, right). For a control, we compared the migratory pattern of endogenous and transferred pDCs. There was no difference in migratory speed within these groups. This was true for application of SFD or HFD, respectively (Supplemental Fig. 2E, 2F). In addition, transferred pDCs increased in FALCs similar to endogenous pDCs when HFD was applied (Supplemental Fig. 2G, 2H). This supports the notion that pDC trafficking and accumulation within FALCs are altered by HFD.

### *Multistep adhesion cascade for pDC homing to the VAT requires P-selectin*

Next, the recruitment of pDCs to VAT, secondary lymphoid organs, and non-lymphoid, yet metabolic active tissue, here the liver, was evaluated in mice with a SFD. pDCs were expanded, harvested, enriched, and labeled before transfer (Supplemental Fig. 3A, 3B). As selectin-mediated tethering and rolling are the first steps of the multistep adhesion cascade in postcapillary venules (48), we inhibited selectin function in short-term adoptive transfer experiments using

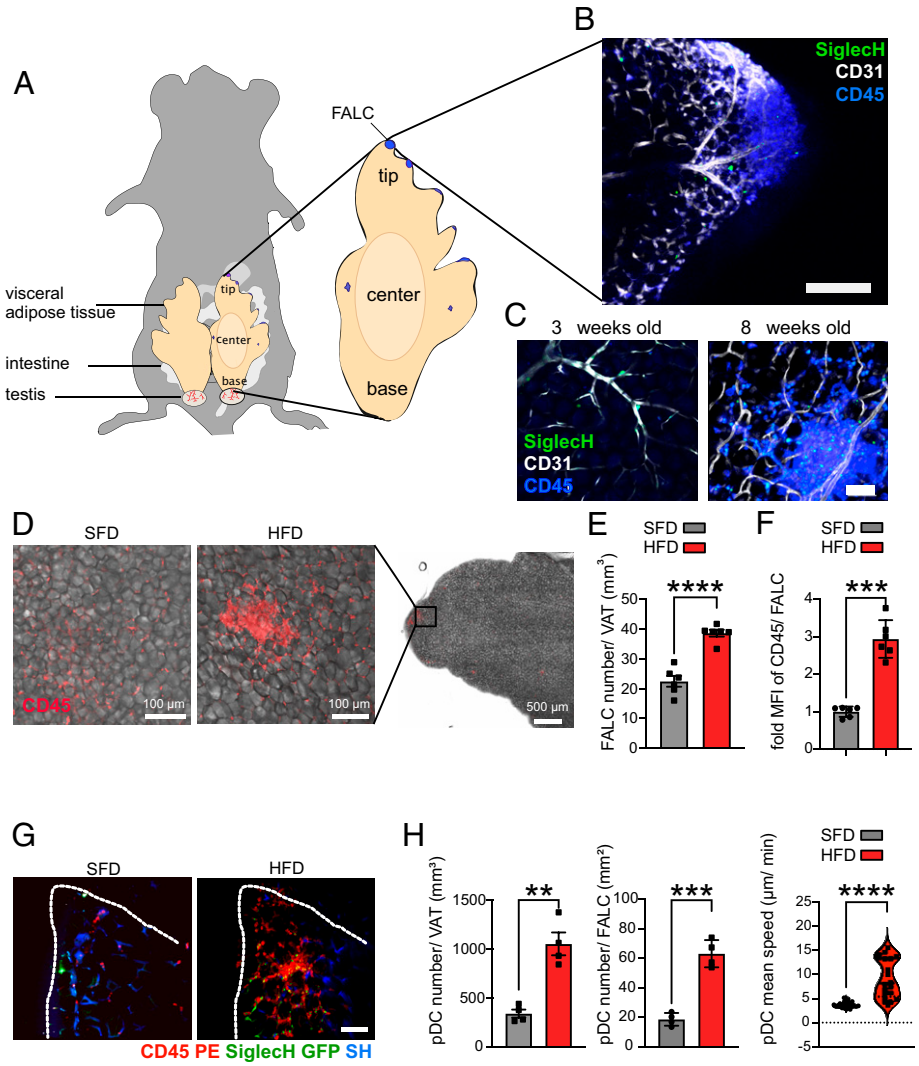


**FIGURE 2.** Diverse distribution of pDCs within the VAT. (**A**) VAT anatomy of the mouse and localization of fat-associated lymphoid clusters (FALCs). Male VAT was separated in the tip area (facing the liver), in the center part, and in the base part, which is attached to testis and epididymis. Confocal microscopy of FALC structures within VAT from chow-treated male mice. (**B**) VAT was stained for SiglecH (pDCs, green), CD31 (endothelia cells, white), and CD45 (hematopoietic cells, blue). Scale bar, 100 µm. (**C**) Representative images of VAT of 3-wk-old (left image) and 8-wk-old male mice (right image) stained for SiglecH (green), CD31 (white), and CD45 (blue). Scale bar, 50 µm. (**D**) Representative images of VAT of SFD or HDF mice, showing the adipocyte tissue in bright field (gray) and $CD45^+$ cells (red). Scale bars, 100 µm. (**E**) Number $CD45^+$ FALCs was quantified per volume of VAT from mice fed with a SFD (gray) and a HFD (red). Each dot represents total number of FALCs of one mouse. (**F**) The maximal MFI of CD45 was measured on the three-dimensional–projection images of FALCs, the mean intensity of SFD samples was set as 1, and the MFI of HFD FALCs was calculated accordingly. (**G**) Representative images of the VAT showing $CD45^+$ cells (red) at the tip of VAT, transferred SiglecH-GFP pDCs (green), and the adipose tissue labeled in blue by the second harmonic generation (SH). Images were acquired by multiphoton microscopy. Scale, 100 µm. (**H**) Left, After 3 wk of SFD and HFD, numbers of pDCs were quantified in relationship to the volume of VAT. (Middle) FALCs were visualized by three-dimensional–maximum projection using Imaris (Bitplane) and numbers of pDCs were quantified per 1 $mm^2$. Right, Mean migratory speed of pDCs was measured by in vivo multiphoton microscopy after 3 wk of a HFD and compared with SFD. $n = 4–5$ mice in each group. Statistical analyses were performed using a Student $t$ test. Values represent mean ± SEM. $^{**}p < 0.05$, $^{***}p < 0.001$, $^{****}p < 0.0001$.

specific function-blocking mAbs (Fig. 3A). PSGL-1, the carbohydrate ligand of P-selectin, was detectable on pDCs (Supplemental Fig. 3C) (49), and blocking P-selectin reduced immigration of pDCs to liver and LNs to some extent (Fig. 3B). The pDC immigration to VAT was completely abolished upon blocking P-selectin, indicating an absolute dependency on P-selectin for pDCs homing to VAT under steady-state conditions (Fig. 3B). In contrast, splenic pDCs did not require P-selectin for immigration (Fig. 3B). As pDCs express and employ L-selectin to home to peripheral LNs (Supplemental Fig. 3C) (50, 51), we blocked L-selectin via MEL-14 mAb treatment. Indeed, the immigration to LNs was significantly reduced (Fig. 3C), but trafficking of pDCs to all other tissues such as liver, spleen, and VAT was not affected (Fig. 3C). Moreover, we did not find any relevance of E-selectin for pDC homing in mice fed with a SFD (Fig. 3D).

### *HFD treatment changes the rolling activity of pDCs in VAT*

To elucidate whether HFD modified the homing process, we studied pDC homing in mice with a SFD or HFD (Fig. 4A). Upon adoptive transfer of pDCs, substantial pDC homing to liver, spleen, and LNs was observed within 18 h (Fig. 4B). Strikingly, VAT of HFD mice showed more immigrated pDCs compared with SFD mice (Fig. 4B). The application of blocking Abs against P-selectin during a HFD reduced homing of pDCs to VAT, albeit in contrast to a SFD, this blockade was not complete (Fig. 4C). Interestingly, after HFD,

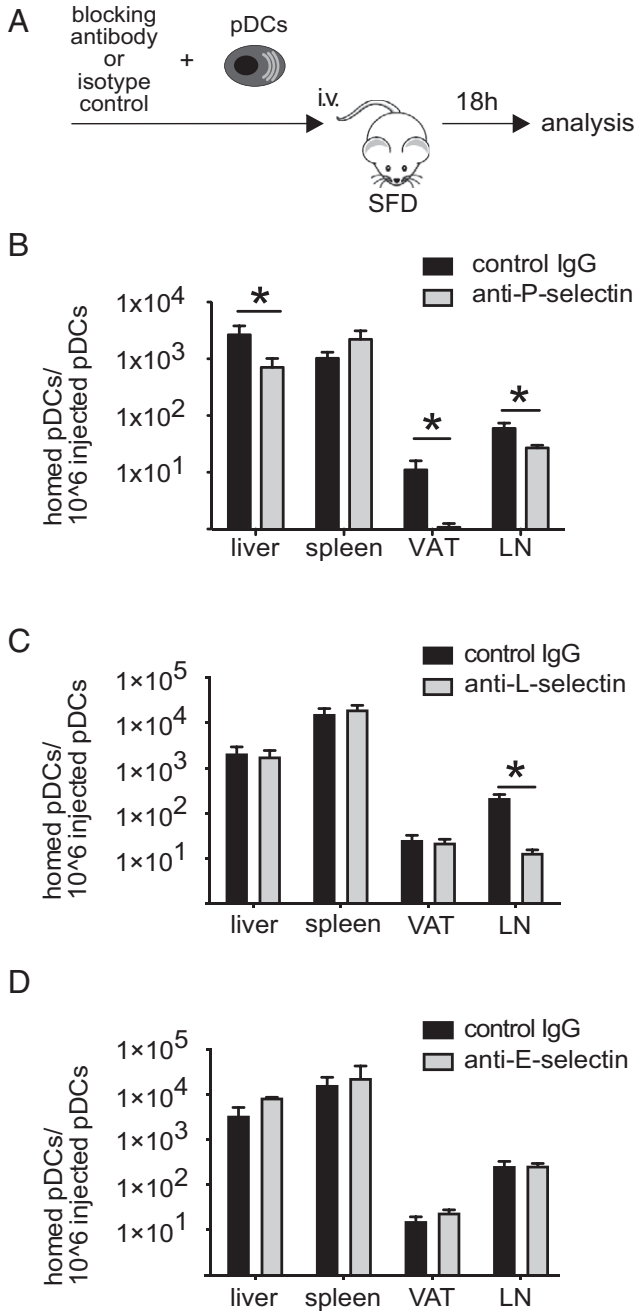


**FIGURE 3.** Homing of pDCs to VAT. (**A**) Scheme for experimental setup for analyzing homing profile of pDCs in SFD-treated recipients. (**B–D**) pDCs were labeled and transferred into mice fed with SFD and that have been additionally treated with isotype control or function-blocking Abs against P-selectin (B), L-selectin (C), and E-selectin (D). After 18 h, liver, spleen, LNs, and VAT were analyzed for immigrated pDCs by flow cytometry. Homed pDCs were calculated per $10^6$ injected pDCs. For (B)–(D), one representative experiment of two is shown. Statistics were performed using a multiple unpaired *t* test. Values represent mean ± SEM. $*p < 0.05$.

L-selectin blockade significantly impaired homing of pDCs to VAT similar to the LNs (Fig. 4D). Moreover, E-selectin, which also did not have any relevance for pDC homing with a SFD (see Fig. 3D), contributed to pDC immigration to VAT, as blocking of E-selectin diminished pDC homing whereas homing to spleen, liver, or LNs was unaffected (Fig. 4E). In line with these findings, the mRNA expression of CD62E specifically increased 50-fold in VAT but not in liver, spleen, and LNs upon HFD compared with a SFD, indicating that high caloric intake alters the molecular signature of VAT (Supplemental Fig. 4A).

*pDC homing to VAT requires integrins and $G_{\alpha i}$ protein signaling*

The next critical step in the multistep adhesion cascade is the transition from rolling to stable arrest, which is mediated by adhesion receptors of the integrin family (52). As pDCs expressed the integrins $\alpha_4\beta_1$ and $\alpha_4\beta_7$ (51, 53) (Supplemental Fig. 3C), we analyzed whether they mediate pDC immigration to VAT. Blocking $\alpha_4\beta_7$ integrins revealed that they are required for pDC homing to VAT but not to liver, spleen, or LNs (Fig. 5A). The blockade of all $\alpha_4$ integrins showed that pDC homing to liver and spleen did not require $\alpha_4$ integrin activity (Fig. 5B) but, as expected (51), the immigration to LNs was reduced by ~50% (Fig. 5B). pDC immigration to VAT was strictly dependent on $\alpha_4$ integrins, as its blockade completely abolished pDC infiltration into VAT (Fig. 5B), indicating that pDC homing to LNs and VAT required $\alpha_4\beta_1$ integrins, but VAT immigration additionally relied on $\alpha_4\beta_7$ integrins. Integrin adhesion requires G protein–coupled receptor (GPCR) signaling, which is sensitive to PTx (54). To decipher the involvement of GPCRs in pDC homing to VAT, competitive homing assays were performed where 50% of pDCs were treated with PTx and coinjected with 50% control pDCs (Fig. 5C, left). Indeed, inhibiting GPCR signaling blocked pDC homing to LNs and, interestingly, also to VAT (Fig. 5C, right), whereas homing to spleen and liver was not affected (Fig. 5C, right). As CCR7 is expressed by pDCs (Supplemental Fig. 3C) and represents a key factor for LN entry via HEVs (34), we performed a competitive homing assay with WT and $CCR7^{-/-}$ pDCs (Fig. 5D). While pDC homing to liver and spleen did not require CCR7, the infiltration to peripheral LNs was significantly reduced as expected (34). Strikingly, the immigration of pDCs to VAT was also inhibited, indicating a necessity of CCR7 signaling for pDC immigration to VAT already with SFD (Fig. 5D). Further treatment with a HFD did not change this requirement (Fig. 5D). Accordingly, qPCR analysis revealed that different CCR7 ligands, namely CCL19, CCL21a, and CCL21b, were expressed in VAT (Supplemental Fig. 4A), pointing toward a role of the CCR7/CCR7 ligand axis. The application of a HFD increased the expression of CCL21a in spleen but not significantly in VAT (Supplemental Fig. 4A). Other chemokine receptors expressed by pDCs such as CXCR3 (Supplemental Fig. 3C) and CCR9 were not essential for pDC homing to VAT, and CCL25 expression was not detected in any organ analyzed (Supplemental Fig. 4B–D). Thus, in addition to $\alpha_4$ integrins, homing of pDCs to VAT involved CCR7 signaling.

*pDC turnover in VAT changes with HFD*

In LNs, pDCs egress to the blood via efferent lymphatics in a S1P-mediated fashion (55). To analyze the number of pDCs that entered VAT, remained there, and potentially egressed to the bloodstream, we measured the number of pDCs in VAT under homeostatic conditions (Fig. 6A, c1) and after daily application of FTY720 for 7 d, resulting in S1PR internalization (Fig. 6A, c2, 6B). FTY720 led to a significant increase in number of pDCs in VAT with a SFD (Fig. 6B), which became 3-fold higher when applied with a HFD (Fig. 6B), indicating that pDC dynamics and turnover in VAT changed with a HFD. Calculating the magnitude from the cell number gained in condition c1 and c2 from SFD and HFD showed that the pDC infiltration was 3-fold higher when mice received additionally a HFD (Fig. 6D, left). To gain further insight into this process, we blocked the infiltration of pDCs to VAT by inhibiting $\alpha_4\beta_7$ integrins (Fig. 6A, R, c3), which led to a decrease in pDC number. The additional treatment with FTY720 (Fig. 6A, c4) revealed an equilibrium of infiltrating and emigrating pDCs under SFD conditions (Fig. 6C, black bars), as it rescued the pDC

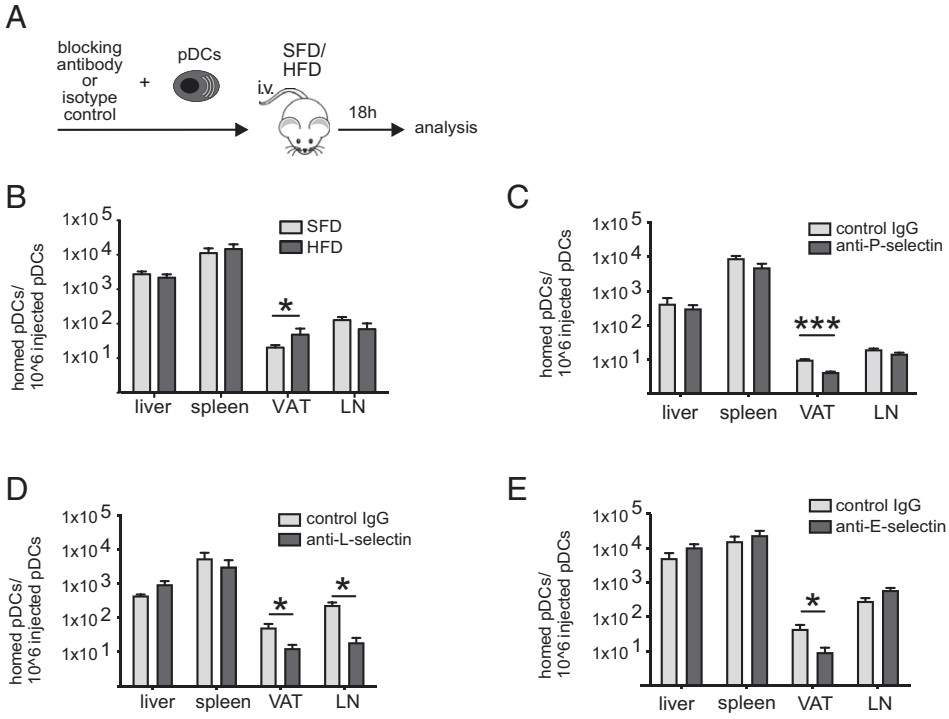


**FIGURE 4.** Homing profile of pDCs in HFD-treated mice. (**A**) Scheme for experimental setup for analyzing homing profile of pDCs during SFD and HFD. (**B**) Labeled pDCs were transferred into mice that had received a SFD or HFD for 3 wk. (**C**–**E**) HFD mice were treated with isotype control or function-blocking Abs against P-selectin (RMP-1) (only here pDCs were derived from in vitro cultures as shown in Supplemental Fig. 4B) (C), L-selectin (MEL-14) (D), or E-selectin (RME-1) (E). After 18 h, liver, spleen, LNs, and VAT were analyzed for immigrated pDCs by flow cytometry. Homed pDCs were calculated per $10^6$ injected pDCs. All groups analyzed consisted of four mice. One representative experiment of two is shown. Values represent mean ± SEM. Statistical analyses were performed using a multiple unpaired *t* test with a two-stage setup (Benjamini, Krieger, and Yekutieli). $*p < 0.05$, $***p < 0.001$.

number to the level seen with isotype control. Upon HFD this changed as the inhibition of pDC infiltration could not decrease the pDC number within the VAT as efficient as with a SFD. Furthermore, the additional blockade of the egress revealed that there was no equilibrium of incoming and emigrating cells anymore (Fig. 6C, red bars). According to the scheme in Fig. 6A, we calculated that the pDC infiltration increased 3-fold within 1 wk of a HFD (Fig. 6D, left), although the egress did not change (Fig. 6D, right) and retention was prolonged (Fig. 6D, middle). Thus, pDC turnover changed dramatically in VAT with a high caloric diet.

### *HFD induces activation of pDCs in VAT*

As a HFD rapidly altered recruitment and turnover of pDCs in VAT as seen in LNs during viral infection (42, 56), we analyzed whether a

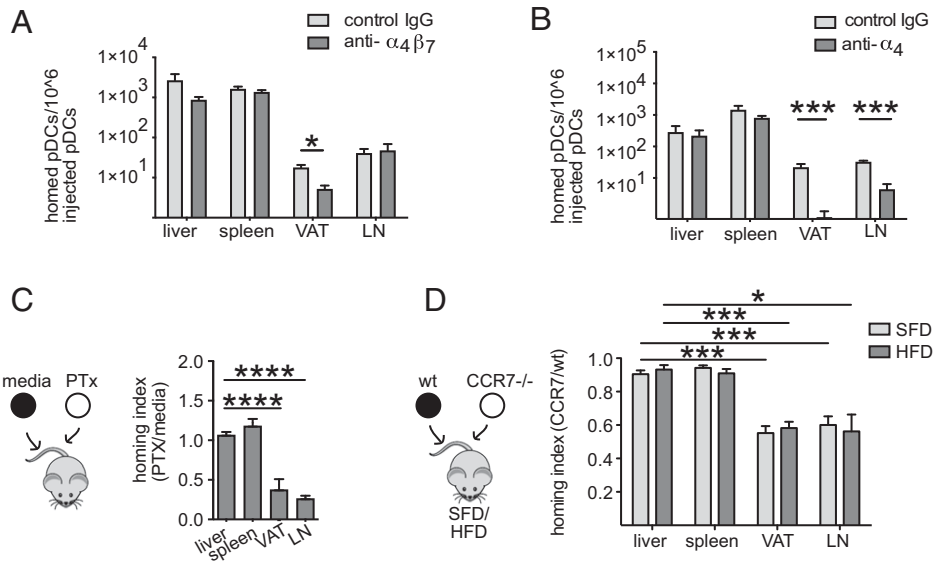


**FIGURE 5.** pDCs require integrin and chemokine signaling to immigrate into VAT. (**A** and **B**) pDC homing to liver, spleen, VAT, and LNs was analyzed by flow cytometry in the presence of (A) $\alpha_4\beta_7$ integrin function-blocking Ab (DATK32) or (B) $\alpha_4$ integrin function-blocking Ab (PS/2) and compared with isotype control Ab-treated mice, accordingly. Statistical analyses were performed using two-way ANOVA with a multiple comparisons test. (**C**) pDCs were enriched and treated ex vivo with media or pertussis toxin (PTx) during cell labeling. pDCs were transferred in equal numbers into recipient mice, and competitive homing was analyzed after 18 h in liver, spleen, VAT, and LNs. The ratio of PTx- and media-treated pDCs was calculated and shown as homing index. (**D**) Competitive homing analysis was performed with WT and CCR7$^{-/-}$ pDCs. Cells were transferred in equal numbers into SFD- or HFD-fed WT mice. Homing index was calculated after 18 h for liver, spleen, LNs, and VAT. For (C) and (D), statistical analyses were performed using a one-way ANOVA with a Tukey multiple comparisons test comparing migration index to corresponding liver values. All groups analyzed consisted of four mice. One representative experiment of two is shown. Values represent means ± SEM. $*p < 0.05$, $**p < 0.01$, $***p < 0.001$, $****p < 0.0001$.

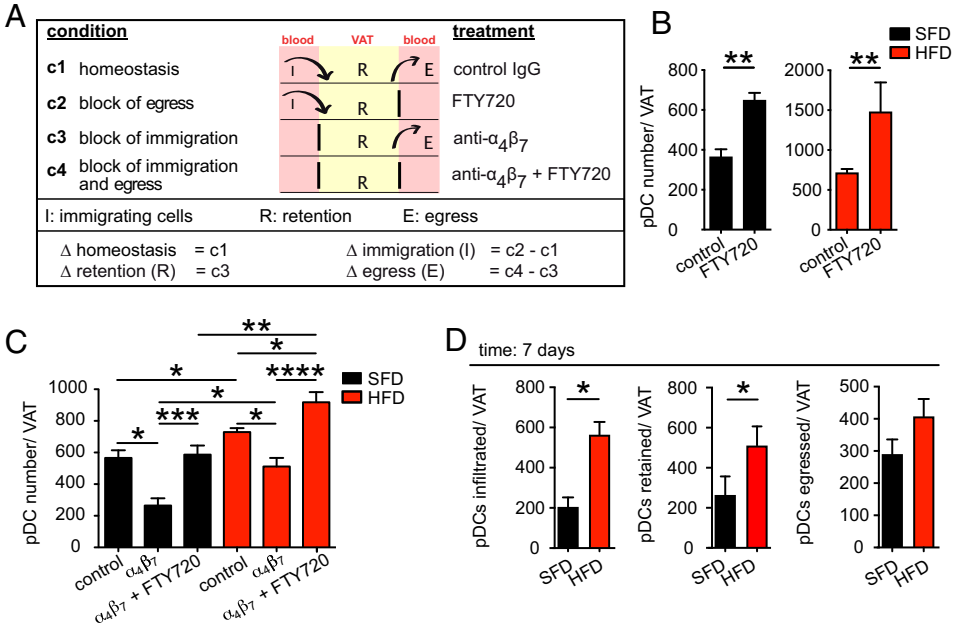


**FIGURE 6.** pDC homeostasis in VAT changes with a HFD. (**A**) Scheme of pDC turnover from blood (pink) to VAT (yellow) and back into blood (pink). "Treatment" indicates the methods used to generate conditions (c1–c4). The analysis measured the immigration (I), retention of pDCs within VAT (R), and the egress of pDCs (E). (**B**) Mice fed with a SFD (black bar) or HFD (red bar) were treated daily for 1 wk with PBS (control) or with FTY720 to block the emigration. VAT was analyzed for pDC number. (**C**) Mice that have been treated for 3 wk with SFD (black bars) or HFD (red bars) were injected daily for the last 7 d with rat IgG2a (control) to measure homeostasis or $\alpha_4\beta_7$ function-blocking Ab to block the immigration of pDCs or with $\alpha_4\beta_7$ function-blocking Ab in combination with FTY720 to block the immigration and emigration activity of pDCs. pDCs of the VAT were measured and counted by flow cytometry. (**D**) pDC infiltration, retention and egress was calculated as indicated in (A) from (B) and (C). All groups analyzed consisted of four to eight mice. Statistical analyses were performed using a Student *t* test (B and D) and one-way ANOVA Tukey multiple comparisons test (C). Values represent mean ± SEM. $*p < 0.05$, $**p < 0.01$, $***p < 0.001$, $****p < 0.0001$.

HFD mediated pDC activation accordingly. Indeed, pDCs in VAT expressed significantly higher levels of activation markers with a HFD compared with a SFD, namely PDC-TREM, CD69, CD86, and CD107, as measured by MFI. The tetraspanin molecule CD9 expression did not change (Fig. 7A, left), suggesting that a HFD did not simply changed pDC composition (57, 58). In contrast, the expression of activation markers of splenic pDCs showed no difference with a HFD versus SFD (Fig. 7A, right), indicating that the change of pDC phenotype upon an obesogenic diet was specific for VAT. As activation of pDCs is usually accompanied by robust IFN-I expression, we measured the expression of IFN-I by pDCs in VAT using MOB mice known to mark IFN-β production by YFP expression (43). In MOB mice fed with SFD, ~20% of all pDCs expressed YFP (Fig. 7B), which increased to >40% with a HFD (Fig. 7B). Furthermore, the intensity of YFP increased with a HFD, indicating an increase of IFN-β expression per pDC (Fig. 7B, right). Accordingly, the absolute amount of IFN-β protein in the VAT was significantly upregulated (Fig. 7C, left). Furthermore, IFN-α was 7-fold upregulated in VAT when a HFD was fed (Fig. 7C, right). In summary, a high-caloric diet specifically activated pDCs in VAT resulting in increased expression of IFN-I. To study the functional impact of pDC trafficking and activation during HFD, we blocked P-selectin by daily injection of a function-blocking Ab (Fig. 7D). Mice receiving isotype control Ab in parallel to a HFD significantly gained body weight starting at day 4 of HFD. In contrast, mice that received a HFD and the P-selectin blocking Ab did not show increased body weight and remained at the level of SFD-treated mice (Fig. 7E). An IPGTT showed that mice treated with HFD in combination with P-selectin blocking Abs had an improved capability to systemically use glucose when compared with isotype-treated HFD-fed mice (Fig. 7F). Furthermore, whereas the weight of VAT in HFD- and isotype-treated mice increased, the treatment with P-selectin blocking Ab during HFD led to reduced weight gain of adipose tissue (Fig. 7G), suggesting that blocking P-selectin can prevent an obesogenic switch at least to some extent upon HFD in our model.

## Discussion

The immune system components within VAT are important and diverse regulators of metabolic processes. They can drive the onset of the metabolic syndrome but may also contribute to its prevention (6, 8, 19). Upon activation, pDCs provide a rapid IFN-I response characterizing the early reaction of the host to disturbances in homeostasis, as described for infections (59). pDCs also respond to metabolic cues as has been shown by increased pDC abundance in VAT of humans with obesity (24). Our comprehensive analysis of pDC distribution in different organs of lean and obese mice revealed a systemic pDC response, with increased numbers in blood, liver, BM, spleen, and VAT upon HFD, with the exception of the LN, as reported earlier (47). In 3-wk-old mice, VAT-resident pDCs were located at the abluminal side of small capillaries even before FALCs were detectable. Accordingly, FALCs start to develop only postnatally (18), whereas secondary lymphoid organs develop during embryogenesis (60, 61). In 8-wk-old mice, however, pDCs were preferentially detectable in FALCs where they showed a similar migratory speed as in LNs under steady-state conditions (56). As FALCs represent lymphoid tissues that orchestrate adaptive immune responses that in turn require pDCs, our results imply a prominent role of these cells in FALC and VAT biology (17, 21, 62). During a HFD, the number of FALCs increased and their volume was enlarged. Furthermore, pDCs within FALCs showed a higher density and an increased migratory speed. To investigate the biology of pDCs, we expanded

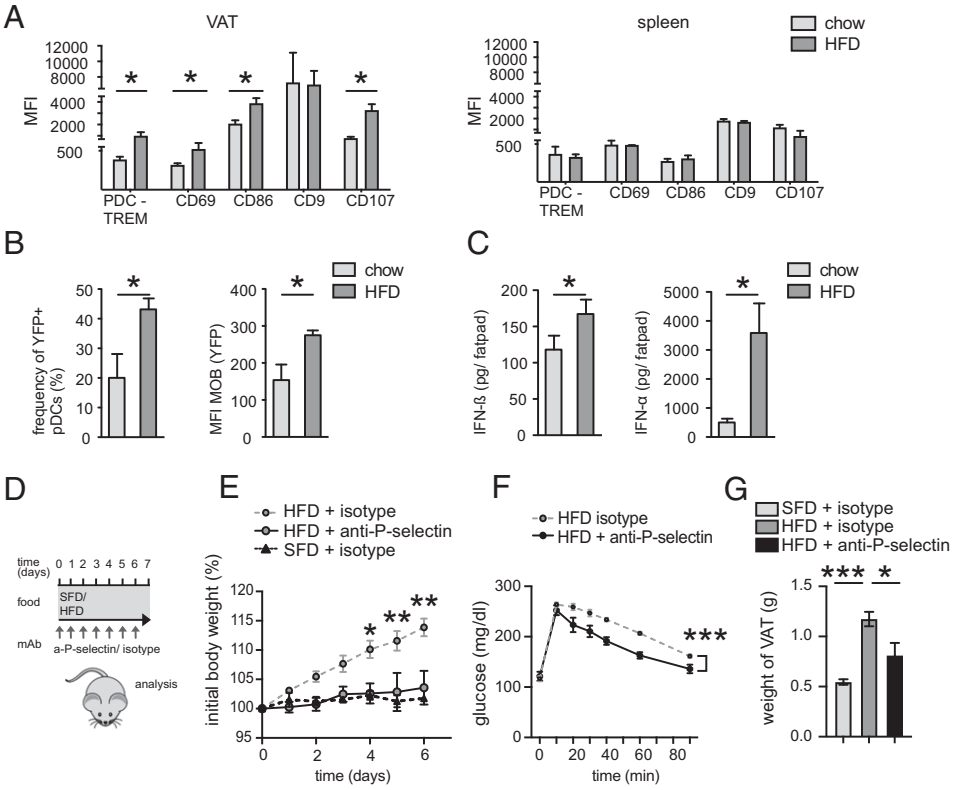


**FIGURE 7.** HFD induces pDC activation in VAT but not in spleen. (**A**) Mice were fed with chow or HFD for 3 wk and pDCs from spleen (left) and VAT (right) were analyzed for expression levels of activation markers by flow cytometry and MFI was calculated. (**B**) MOB mice were fed with chow or HFD for 3 wk and pDCs in VAT were analyzed for YFP expression by flow cytometry. (**C**) IFN-β and IFN-$\alpha_{(1+4)}$ of VAT from chow- or HFD-fed mice were measured by ELISA. (**D**) Scheme of experimental setup. Mice were fed with SFD (black line) or HFD and daily injected i.p. with isotype (gray dotted line) or mAb blocking P-selectin (RMP-1) (back dotted line) for 7 d. (**E**) Body weight was measured daily, and percent of weight gain was calculated from initial body weight. (**F**) An IPGTT was performed. Mice had been starved for 5 h and 1 g/kg glucose had been injected i.p. Blood glucose was measured at indicated time points. (**G**) Weight of VAT was measured for mice described in (D). All groups analyzed consisted of four to six mice from two independent experiments. Statistical analyses were performed with a one-way ANOVA multiple comparison test (A and G), Student *t* test (B and C), or two-way ANOVA (E and F). Values represent means ± SEM. $*p < 0.05$, $**p < 0.01$, $***p < 0.001$.

the pDC population using the B16-FLT3L system, as the endogenous pDC number was too low to perform homing experiments. This approach has been widely used in earlier studies to analyze the function and homing of pDCs (33, 34). Moreover, we showed that the expression profile of adhesion molecules of FLT3L-expanded pDCs (Supplemental Fig. 3C) was similar to the molecular signature of adhesion molecules expressed by endogenous pDCs, demonstrating their suitability for our studies. The homing of pDCs to VAT required P-selectin already under normal conditions, indicating that the VAT milieu differs from other peripheral organs (63). In contrast, E-selectin was not employed by pDCs under normal conditions but with HFD. The involvement of E-selectin in pDC recruitment to VAT but not to LNs suggests that 3 wk of a HFD were sufficient to cause an inflammatory state in VAT, whereas the peripheral LN was spared. This was confirmed by the fact that we found a substantial increase of E-selectin mRNA expression specifically in VAT upon a HFD compared with a SFD but not in other organs, including liver, spleen, and LNs. Whereas P-selectin can be prestored in Weibel–Palade bodies of endothelial cells, E-selectin is expressed de novo upon stimulation by inflammatory mediators (49, 64). In addition, L-selectin was expressed by pDCs but it was not required for pDCs homing to VAT under normal conditions. However, L-selectin became important with a HFD when VAT is remodeled (65). Interestingly, the expression profile of homing molecules on pDCs, including PSGL-1, CD62L, CD49d, $\alpha_4\beta_7$, and CCR7, was largely unaffected by HFD (data not shown), suggesting that rather a switch of VAT toward an inflammatory milieu than a pDC-intrinsic mechanism mediates increased pDC homing to and retention in VAT (20, 66).

Two of the most relevant adhesion molecules for leukocyte homing are $\alpha_4\beta_1$ and $\alpha_4\beta_7$ integrins, and we confirmed their expression by pDCs (51, 67). Whereas homing of pDCs to LN involved $\alpha_4\beta_1$ integrins only, the VAT infiltration additionally relied on $\alpha_4\beta_7$ integrins, usually employed for pDC homing to the gut (68). Integrin activation requires $G_{\alpha i}$-mediated PTx-sensitive signaling and, indeed, the treatment with PTx prevented pDC infiltration to VAT and LNs, indicating an essential $G_{\alpha i}$ signaling for this recruitment process.

pDCs expressed CCR7, which signals via $G\alpha_i$, and identical to LN homing, pDCs required CCR7 signaling to infiltrate VAT during SFD and HFD. Gene expression analyses revealed expression of CCR7 ligands within spleen, LNs, and VAT, suggesting a functional role of this chemokine receptor axis under both conditions. Although pDCs express CCR9 (33, 69), mRNA expression of its ligand CCL25 could not be identified. However, chemokines do not require local gene expression, as they can be transported and presented via glycosaminoglycans, but CCR9 engagement for pDC homing to VAT, spleen, liver, and LNs as shown for thymus and gut (33, 70) could not be observed. Similarly, CXCR3 signaling was not involved in pDC homing to VAT, but may be required for inner tissue migration as shown for intranodal positioning within the LN (71).

Studying pDC dynamics in VAT revealed that a HFD led to a rise in pDC number in VAT, and blocking the egress with FTY720 further resulted in a 3-fold increase, indicating that pDCs actively

left the VAT via a S1P-dependent mechanism. Moreover, our data indicated an equilibrium of pDC influx and efflux under homeostatic conditions with SFD. A HFD increased the number of infiltrating pDCs and prolonged their retention, resulting in a rise of total pDC number in VAT. In addition, pDCs showed a higher expression of the early activation marker CD69 with a HFD. For activated T cells in the LN, it has been demonstrated that CD69 physically interacts with S1PR, resulting in downregulation of S1PR surface expression and thereby blocking S1P-mediated T cell egress (72). Although obese humans present elevated S1P levels in the blood (73), we did not find an increased egress of pDCs from VAT, which may be due to their upregulated CD69 expression with HFD. In LNs, higher retention times of pDCs coincide with a change to an activated phenotype (55). Indeed, VAT pDCs displayed an activated phenotype with a HFD. Moreover, 20% of all pDCs expressed IFN-I in the steady state, which was similar to pDCs in other peripheral tissues (43), whereas obesogenic diet increased IFN-I expression by pDCs up to 40% in VAT. IFN-I in turn contributes to the polarization of M2 macrophages to M1 macrophages, thereby promoting proinflammatory cytokine release and fueling meta-inflammation, leading to systemic insulin resistance (24).

Thus, pDCs reside preferentially in FALCs of VAT in adult mice under steady-state conditions and display increased homing to and retention in VAT after 3 wk of HFD, resulting in an accumulation of pDCs caused by a shift of VAT toward an inflammatory state as outlined by dramatically increased E-selectin expression. In vivo imaging showed an increase of migratory speed after high caloric intake, indicating a transition from a rather stationary to scanning mode within the FALCs. The dramatic disturbances of trafficking with a HFD coincide with an activation of pDCs and increased IFN-I expression in VAT, suggesting a potential mechanistic link by which IFN-I may render VAT into a chronic inflammatory tissue (41).

This hitherto unknown modulation of pDC homeostasis by a HFD may shed new light on the impact of our daily diet on the complex interplay between the immune system and adipose tissue, a topic that is of great clinical importance. Interestingly, the genetic abrogation of IFN-I signaling prevents the development of obesity (22), identifying pDCs as a potentially powerful target to treat obesity. Recently, IFN-I from pDCs in VAT has been demonstrated to fuel the loss of VAT-resident regulatory T cells that results in an obesogenic phenotype (41). Furthermore, the blockade of pDC infiltration into VAT by P-selectin blockade in combination with a HFD prevented gain of body weight and improved glucose tolerance at least during the first week of high caloric intake. Thus, pDC trafficking may represent an interesting target for therapeutic intervention in obesity by preventing weight gain and the metabolic syndrome.

## Acknowledgments

We thank Michael Flynn for assistance performing animal experiments, Wolfgang Kastenmüller for providing reagents and the ubiquitin C−tdTomato mice, and Stefanie Scheu for providing mice. We acknowledge the Core Facility Flow Cytometry at the Biomedical Center, Ludwig-Maximilians-Universität München for providing FACS equipment and the Multiphoton Imaging Core Facility at the Walter Brendel Center for Experimental Medicine.

## Disclosures

The authors have no financial conflicts of interest.

## References

1. Tremmel, M., U. G. Gerdtham, P. M. Nilsson, and S. Saha. 2017. Economic burden of obesity: a systematic literature review. *Int. J. Environ. Res. Public Health* 14: 435.
2. Ahima, R. S., and J. S. Flier. 2000. Adipose tissue as an endocrine organ. *Trends Endocrinol. Metab.* 11: 327–332.
3. Sun, K., C. M. Kusminski, and P. E. Scherer. 2011. Adipose tissue remodeling and obesity. *J. Clin. Invest.* 121: 2094–2101.
4. Maraskovsky, E., K. Brasel, M. Teepe, E. R. Roux, S. D. Lyman, K. Shortman, and H. J. McKenna. 1996. Dramatic increase in the numbers of functionally mature dendritic cells in Flt3 ligand-treated mice: multiple dendritic cell subpopulations identified. *J. Exp. Med.* 184: 1953–1962.
5. Macdougall, C. E., E. G. Wood, J. Loschko, V. Scagliotti, F. C. Cassidy, M. E. Robinson, N. Feldhahn, L. Castellano, M. B. Voisin, F. Marelli-Berg, et al. 2018. Visceral adipose tissue immune homeostasis is regulated by the crosstalk between adipocytes and dendritic cell subsets. *Cell Metab.* 27: 588–601.e4.
6. Lynch, L., M. Nowak, B. Varghese, J. Clark, A. E. Hogan, V. Toxavidis, S. P. Balk, D. O'Shea, C. O'Farrelly, and M. A. Exley. 2012. Adipose tissue invariant NKT cells protect against diet-induced obesity and metabolic disorder through regulatory cytokine production. *Immunity* 37: 574–587.
7. Carolan, E., L. M. Tobin, B. A. Mangan, M. Corrigan, G. Gaoatswe, G. Byrne, J. Geoghegan, D. Cody, J. O'Connell, D. C. Winter, et al. 2015. Altered distribution and increased IL-17 production by mucosal-associated invariant T cells in adult and childhood obesity. *J. Immunol.* 194: 5775–5780.
8. Priceman, S. J., M. Kujawski, S. Shen, G. A. Cherryholmes, H. Lee, C. Zhang, L. Kruper, J. Mortimer, R. Jove, A. D. Riggs, and H. Yu. 2013. Regulation of adipose tissue T cell subsets by Stat3 is crucial for diet-induced obesity and insulin resistance. *Proc. Natl. Acad. Sci. USA* 110: 13079–13084.
9. Brestoff, J. R., B. S. Kim, S. A. Saenz, R. R. Stine, L. A. Monticelli, G. F. Sonnenberg, J. J. Thome, D. L. Farber, K. Lutfy, P. Seale, and D. Artis. 2015. Group 2 innate lymphoid cells promote beiging of white adipose tissue and limit obesity. *Nature* 519: 242–246.
10. Khan, T., E. S. Muise, P. Iyengar, Z. V. Wang, M. Chandalia, N. Abate, B. B. Zhang, P. Bonaldo, S. Chua, and P. E. Scherer. 2009. Metabolic dysregulation and adipose tissue fibrosis: role of collagen VI. *Mol. Cell. Biol.* 29: 1575–1591.
11. Wentworth, J. M., G. Naselli, W. A. Brown, L. Doyle, B. Phipson, G. K. Smyth, M. Wabitsch, P. E. O'Brien, and L. C. Harrison. 2010. Pro-inflammatory $CD11c^+CD206^+$ adipose tissue macrophages are associated with insulin resistance in human obesity. *Diabetes* 59: 1648–1656.
12. Mauer, J., J. L. Denson, and J. C. Brüning. 2015. Versatile functions for IL-6 in metabolism and cancer. *Trends Immunol.* 36: 92–101.
13. Schipper, H. S., B. Prakken, E. Kalkhoven, and M. Boes. 2012. Adipose tissue-resident immune cells: key players in immunometabolism. *Trends Endocrinol. Metab.* 23: 407–415.
14. Fontana, L., J. C. Eagon, M. E. Trujillo, P. E. Scherer, and S. Klein. 2007. Visceral fat adipokine secretion is associated with systemic inflammation in obese humans. *Diabetes* 56: 1010–1013.
15. Caër, C., C. Rouault, T. Le Roy, C. Poitou, J. Aron-Wisnewsky, A. Torcivia, J. C. Bichet, K. Clément, M. Guerre-Millo, and S. André. 2017. Immune cell-derived cytokines contribute to obesity-related inflammation, fibrogenesis and metabolic deregulation in human adipose tissue. *Sci. Rep.* 7: 3000.
16. Chusyd, D. E., D. Wang, D. M. Huffman, and T. R. Nagy. 2016. Relationships between rodent white adipose fat pads and human white adipose fat depots. *Front. Nutr.* 3: 10.
17. Moro, K., T. Yamada, M. Tanabe, T. Takeuchi, T. Ikawa, H. Kawamoto, J. Furusawa, M. Ohtani, H. Fujii, and S. Koyasu. 2010. Innate production of $T_H2$ cytokines by adipose tissue-associated c-$Kit^+Sca\text{-}1^+$ lymphoid cells. *Nature* 463: 540–544.
18. Bénézech, C., N. T. Luu, J. A. Walker, A. A. Kruglov, Y. Loo, K. Nakamura, Y. Zhang, S. Nayar, L. H. Jones, A. Flores-Langarica, et al. 2015. Inflammation-induced formation of fat-associated lymphoid clusters. *Nat. Immunol.* 16: 819–828.
19. Winer, D. A., S. Winer, L. Shen, P. P. Wadia, J. Yantha, G. Paltser, H. Tsui, P. Wu, M. G. Davidson, M. N. Alonso, et al. 2011. B cells promote insulin resistance through modulation of T cells and production of pathogenic IgG antibodies. *Nat. Med.* 17: 610–617.
20. Rangel-Moreno, J., J. E. Moyron-Quiroz, D. M. Carragher, K. Kusser, L. Hartson, A. Moquin, and T. D. Randall. 2009. Omental milky spots develop in the absence of lymphoid tissue-inducer cells and support B and T cell responses to peritoneal antigens. *Immunity* 30: 731–743.
21. Jackson-Jones, L. H., S. M. Duncan, M. S. Magalhaes, S. M. Campbell, R. M. Maizels, H. J. McSorley, J. E. Allen, and C. Bénézech. 2016. Fat-associated lymphoid clusters control local IgM secretion during pleural infection and lung inflammation. *Nat. Commun.* 7: 12651.
22. Hannibal, T. D., A. Schmidt-Christensen, J. Nilsson, N. Fransén-Pettersson, L. Hansen, and D. Holmberg. 2017. Deficiency in plasmacytoid dendritic cells and type I interferon signalling prevents diet-induced obesity and insulin resistance in mice. *Diabetologia* 60: 2033–2041.
23. Stefanovic-Racic, M., X. Yang, M. S. Turner, B. S. Mantell, D. B. Stolz, T. L. Sumpter, I. J. Sipula, N. Dedousis, D. K. Scott, P. A. Morel, et al. 2012. Dendritic cells promote macrophage infiltration and comprise a substantial proportion of obesity-associated increases in $CD11c^+$ cells in adipose tissue and liver. *Diabetes* 61: 2330–2339.
24. Ghosh, A. R., R. Bhattacharya, S. Bhattacharya, T. Nargis, O. Rahaman, P. Duttagupta, D. Raychaudhuri, C. S. Liu, S. Roy, P. Ghosh, et al. 2016. Adipose recruitment and activation of plasmacytoid dendritic cells fuel metaflammation. *Diabetes* 65: 3440–3452.
25. Liu, Y. J. 2005. IPC: professional type 1 interferon-producing cells and plasmacytoid dendritic cell precursors. *Annu. Rev. Immunol.* 23: 275–306.
26. Reizis, B., A. Bunin, H. S. Ghosh, K. L. Lewis, and V. Sisirak. 2011. Plasmacytoid dendritic cells: recent progress and open questions. *Annu. Rev. Immunol.* 29: 163–183.

27. Honda, K., Y. Ohba, H. Yanai, H. Negishi, T. Mizutani, A. Takaoka, C. Taya, and T. Taniguchi. 2005. Spatiotemporal regulation of MyD88-IRF-7 signalling for robust type-I interferon induction. *Nature* 434: 1035–1040.
28. Crozat, K., R. Guiton, M. Guilliams, S. Henri, T. Baranek, I. Schwartz-Cornil, B. Malissen, and M. Dalod. 2010. Comparative genomics as a tool to reveal functional equivalences between human and mouse dendritic cell subsets. *Immunol. Rev.* 234: 177–198.
29. Colonna, M., G. Trinchieri, and Y. J. Liu. 2004. Plasmacytoid dendritic cells in immunity. *Nat. Immunol.* 5: 1219–1226.
30. Penna, G., S. Sozzani, and L. Adorini. 2001. Cutting edge: selective usage of chemokine receptors by plasmacytoid dendritic cells. *J. Immunol.* 167: 1862–1866.
31. Sozzani, S., W. Vermi, A. Del Prete, and F. Facchetti. 2010. Trafficking properties of plasmacytoid dendritic cells in health and disease. *Trends Immunol.* 31: 270–277.
32. Yoneyama, H., K. Matsuno, Y. Zhang, T. Nishiwaki, M. Kitabatake, S. Ueha, S. Narumi, S. Morikawa, T. Ezaki, B. Lu, et al. 2004. Evidence for recruitment of plasmacytoid dendritic cell precursors to inflamed lymph nodes through high endothelial venules. *Int. Immunol.* 16: 915–928.
33. Wendland, M., N. Czeloth, N. Mach, B. Malissen, E. Kremmer, O. Pabst, and R. Förster. 2007. CCR9 is a homing receptor for plasmacytoid dendritic cells to the small intestine. *Proc. Natl. Acad. Sci. USA* 104: 6347–6352.
34. Seth, S., L. Oberdörfer, R. Hyde, K. Hoff, V. Thies, T. Worbs, S. Schmitz, and R. Förster. 2011. CCR7 essentially contributes to the homing of plasmacytoid dendritic cells to lymph nodes under steady-state as well as inflammatory conditions. *J. Immunol.* 186: 3364–3372.
35. Dillmann, C., J. Mora, C. Olesch, B. Brüne, and A. Weigert. 2015. S1PR4 is required for plasmacytoid dendritic cell differentiation. *Biol. Chem.* 396: 775–782.
36. Spiegel, S., and S. Milstien. 2011. The outs and the ins of sphingosine-1-phosphate in immunity. *Nat. Rev. Immunol.* 11: 403–415.
37. Pinschewer, D. D., A. F. Ochsenbein, B. Odermatt, V. Brinkmann, H. Hengartner, and R. M. Zinkernagel. 2000. FTY720 immunosuppression impairs effector T cell peripheral homing without affecting induction, expansion, and memory. *J. Immunol.* 164: 5761–5770.
38. Mandala, S., R. Hajdu, J. Bergstrom, E. Quackenbush, J. Xie, J. Milligan, R. Thornton, G. J. Shei, D. Card, C. Keohane, et al. 2002. Alteration of lymphocyte trafficking by sphingosine-1-phosphate receptor agonists. *Science* 296: 346–349.
39. Gilliet, M., W. Cao, and Y. J. Liu. 2008. Plasmacytoid dendritic cells: sensing nucleic acids in viral infection and autoimmune diseases. *Nat. Rev. Immunol.* 8: 594–606.
40. Kim, S. J., Y. Choi, Y. H. Choi, and T. Park. 2012. Obesity activates toll-like receptor-mediated proinflammatory signaling cascades in the adipose tissue of mice. *J. Nutr. Biochem.* 23: 113–122.
41. Li, C., G. Wang, P. Sivasami, R. N. Ramirez, Y. Zhang, C. Benoist, and D. Mathis. 2021. Interferon-α-producing plasmacytoid dendritic cells drive the loss of adipose tissue regulatory T cells during obesity. *Cell Metab.* 33: 1610–1623.e5.
42. Swiecki, M., S. Gilfillan, W. Vermi, Y. Wang, and M. Colonna. 2010. Plasmacytoid dendritic cell ablation impacts early interferon responses and antiviral NK and $CD8^+$ T cell accrual. *Immunity* 33: 955–966.
43. Scheu, S., P. Dresing, and R. M. Locksley. 2008. Visualization of IFNβ production by plasmacytoid versus conventional dendritic cells under specific stimulation conditions in vivo. *Proc. Natl. Acad. Sci. USA* 105: 20416–20421.
44. Shi, G. P., J. A. Villadangos, G. Dranoff, C. Small, L. Gu, K. J. Haley, R. Riese, H. L. Ploegh, and H. A. Chapman. 1999. Cathepsin S required for normal MHC class II peptide loading and germinal center development. *Immunity* 10: 197–206.
45. Gallatin, W. M., I. L. Weissman, and E. C. Butcher. 1983. A cell-surface molecule involved in organ-specific homing of lymphocytes. *Nature* 304: 30–34.
46. Swiecki, M., Y. Wang, E. Riboldi, A. H. Kim, A. Dzutsev, S. Gilfillan, W. Vermi, C. Ruedl, G. Trinchieri, and M. Colonna. 2014. Cell depletion in mice that express diphtheria toxin receptor under the control of SiglecH encompasses more than plasmacytoid dendritic cells. *J. Immunol.* 192: 4409–4416.
47. Kim, C. S., S. C. Lee, Y. M. Kim, B. S. Kim, H. S. Choi, T. Kawada, B. S. Kwon, and R. Yu. 2008. Visceral fat accumulation induced by a high-fat diet causes the atrophy of mesenteric lymph nodes in obese mice. *Obesity (Silver Spring)* 16: 1261–1269.
48. Ley, K., C. Laudanna, M. I. Cybulsky, and S. Nourshargh. 2007. Getting to the site of inflammation: the leukocyte adhesion cascade updated. *Nat. Rev. Immunol.* 7: 678–689.
49. Vestweber, D., and J. E. Blanks. 1999. Mechanisms that regulate the function of the selectins and their ligands. *Physiol. Rev.* 79: 181–213.
50. Nakano, H., M. Yanagita, and M. D. Gunn. 2001. $CD11c^+B220^+Gr\text{-}1^+$ cells in mouse lymph nodes and spleen display characteristics of plasmacytoid dendritic cells. *J. Exp. Med.* 194: 1171–1178.
51. Matsutani, T., T. Tanaka, K. Tohya, K. Otani, M. H. Jang, E. Umemoto, K. Taniguchi, H. Hayasaka, K. Ueda, and M. Miyasaka. 2007. Plasmacytoid dendritic cells employ multiple cell adhesion molecules sequentially to interact with high endothelial venule cells—molecular basis of their trafficking to lymph nodes. *Int. Immunol.* 19: 1031–1037.
52. Takada, Y., X. Ye, and S. Simon. 2007. The integrins. *Genome Biol.* 8: 215.
53. Ahima, R. S., and M. A. Lazar. 2008. Adipokines and the peripheral and neural control of energy balance. *Mol. Endocrinol.* 22: 1023–1031.
54. Murphy, P. M. 1994. The molecular biology of leukocyte chemoattractant receptors. *Annu. Rev. Immunol.* 12: 593–633.
55. Gao, Y., B. Majchrzak-Kita, E. N. Fish, and J. L. Gommerman. 2009. Dynamic accumulation of plasmacytoid dendritic cells in lymph nodes is regulated by interferon-β. *Blood* 114: 2623–2631.
56. Brewitz, A., S. Eickhoff, S. Dähling, T. Quast, S. Bedoui, R. A. Kroczek, C. Kurts, N. Garbi, W. Barchet, M. Iannacone, et al. 2017. $CD8^+$ T cells orchestrate $pDC\text{-}XCR1^+$ dendritic cell spatial and functional cooperativity to optimize priming. *Immunity* 46: 205–219.
57. Björck, P., H. X. Leong, and E. G. Engleman. 2011. Plasmacytoid dendritic cell dichotomy: identification of IFN-α producing cells as a phenotypically and functionally distinct subset. *J. Immunol.* 186: 1477–1485.
58. Musumeci, A., K. Lutz, E. Winheim, and A. B. Krug. 2019. What makes a pDC: recent advances in understanding plasmacytoid DC development and heterogeneity. *Front. Immunol.* 10: 1222.
59. Wang, B. X., and E. N. Fish. 2012. The yin and yang of viruses and interferons. *Trends Immunol.* 33: 190–197.
60. Adachi, S., H. Yoshida, K. Honda, K. Maki, K. Saijo, K. Ikuta, T. Saito, and S. I. Nishikawa. 1998. Essential role of IL-7 receptor alpha in the formation of Peyer's patch anlage. *Int. Immunol.* 10: 1–6.
61. Nishikawa, S., K. Honda, P. Vieira, and H. Yoshida. 2003. Organogenesis of peripheral lymphoid organs. *Immunol. Rev.* 195: 72–80.
62. Jackson-Jones, L. H., and C. Bénézech. 2018. Control of innate-like B cell location for compartmentalised IgM production. *Curr. Opin. Immunol.* 50: 9–13.
63. Schäffler, A., and J. Schölmerich. 2010. Innate immunity and adipose tissue biology. *Trends Immunol.* 31: 228–235.
64. Collins, T., M. A. Read, A. S. Neish, M. Z. Whitley, D. Thanos, and T. Maniatis. 1995. Transcriptional regulation of endothelial cell adhesion molecules: NF-κB and cytokine-inducible enhancers. *FASEB J.* 9: 899–909.
65. Strissel, K. J., Z. Stancheva, H. Miyoshi, J. W. Perfield II, J. DeFuria, Z. Jick, A. S. Greenberg, and M. S. Obin. 2007. Adipocyte death, adipose tissue remodeling, and obesity complications. *Diabetes* 56: 2910–2918.
66. Reilly, S. M., and A. R. Saltiel. 2017. Adapting to obesity with adipose tissue inflammation. *Nat. Rev. Endocrinol.* 13: 633–643.
67. Garnier, A., S. Laffont, L. Garnier, E. Kaba, U. Deutsch, B. Engelhardt, and J. C. Guéry. 2019. CD49d/CD29-integrin controls the accumulation of plasmacytoid dendritic cells into the CNS during neuroinflammation. *Eur. J. Immunol.* 49: 2030–2043.
68. Meenan, J., J. Spaans, T. A. Grool, S. T. Pals, G. N. Tytgat, and S. J. van Deventer. 1997. Altered expression of alpha 4 beta 7, a gut homing integrin, by circulating and mucosal T cells in colonic mucosal inflammation. *Gut* 40: 241–246.
69. Hadeiba, H., T. Sato, A. Habtezion, C. Oderup, J. Pan, and E. C. Butcher. 2008. CCR9 expression defines tolerogenic plasmacytoid dendritic cells able to suppress acute graft-versus-host disease. *Nat. Immunol.* 9: 1253–1260.
70. Hadeiba, H., K. Lahl, A. Edalati, C. Oderup, A. Habtezion, R. Pachynski, L. Nguyen, A. Ghodsi, S. Adler, and E. C. Butcher. 2012. Plasmacytoid dendritic cells transport peripheral antigens to the thymus to promote central tolerance. *Immunity* 36: 438–450.
71. Vanbervliet, B., N. Bendriss-Vermare, C. Massacrier, B. Homey, O. de Bouteiller, F. Brière, G. Trinchieri, and C. Caux. 2003. The inducible CXCR3 ligands control plasmacytoid dendritic cell responsiveness to the constitutive chemokine stromal cell-derived factor 1 (SDF-1)/CXCL12. *J. Exp. Med.* 198: 823–830.
72. Shiow, L. R., D. B. Rosen, N. Brdicková, Y. Xu, J. An, L. L. Lanier, J. G. Cyster, and M. Matloubian. 2006. CD69 acts downstream of interferon-alpha/beta to inhibit S1P1 and lymphocyte egress from lymphoid organs. *Nature* 440: 540–544.
73. Ito, S., S. Iwaki, K. Koike, Y. Yuda, A. Nagasaki, R. Ohkawa, Y. Yatomi, T. Furumoto, H. Tsutsui, B. E. Sobel, and S. Fujii. 2013. Increased plasma sphingosine-1-phosphate in obese individuals and its capacity to increase the expression of plasminogen activator inhibitor-1 in adipocytes. *Coron. Artery Dis.* 24: 642–650.

# Supplementary Figures

**Supplementary Figure 1**

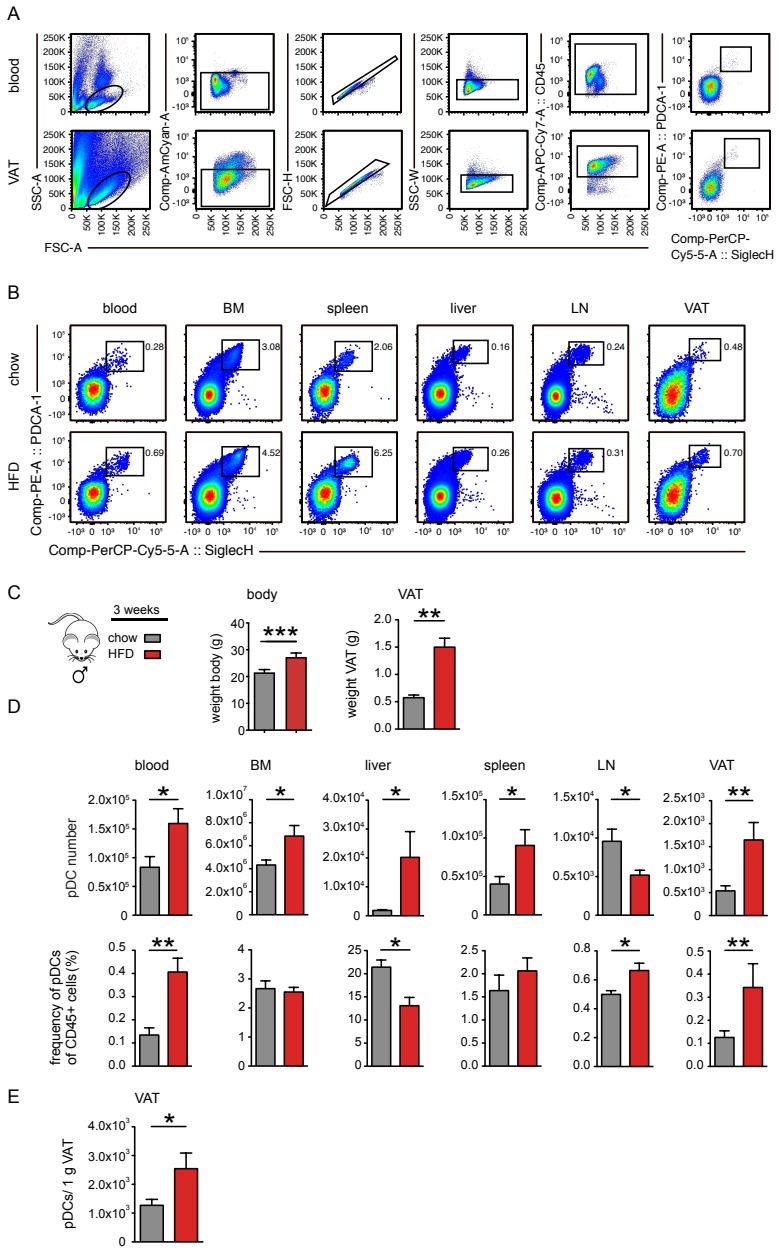


SUPPLEMENTAL FIGURE 1. **pDC gating strategy from blood, peripheral and lymphoid organs.** (**A**) Gating strategy for PDCA-1+SiglecH+ cells (pDCs) in blood and single cell suspensions of peripheral and lymphoid organs from mice after three weeks of standard chow diet (chow) or high fat diet (HFD). Representative gating strategies for blood (upper panel) and VAT (lower panel) from mice with chow are shown. (**B**) Blood and single cell suspensions of peripheral and lymphoid organs were obtained from mice fed for three weeks with chow or HFD and were analyzed for pDCs (PDCA-1+SiglecH+) using flow cytometry (gating strategy in *A*). Numbers indicate pDC frequency as percentage of CD45+ cells (100%). Representative pseudocolor dot plots are shown. (A-B) One representative is shown. (C-E) Male mice were fed for three weeks with normal standard chow (black bars) or high fat diet (HFD, red bars) and weight of VAT was measured (**C**). (**D**) Blood and single cell suspensions of different peripheral and lymphoid tissues of mice were analyzed by flow cytometry. BM, bone marrow; LN, inguinal lymph node; VAT, visceral adipose tissue. Absolute pDC numbers were calculated per 1 ml blood or per organ or femur and pDC frequency was calculated as percentage of CD45+ cells (100%). (**E**) pDC numbers per 1 g VAT (from *C* and *D)* were calculated. (C-E) The animal experiment was repeated twice with 3-4 animals per group and similar outcome. One representative experiment is shown. Statistics were performed using Student's *t*-test. Values represent mean ± SEM. *$p < 0.05$; **$p < 0.01$.

**Supplemental Figure 2**

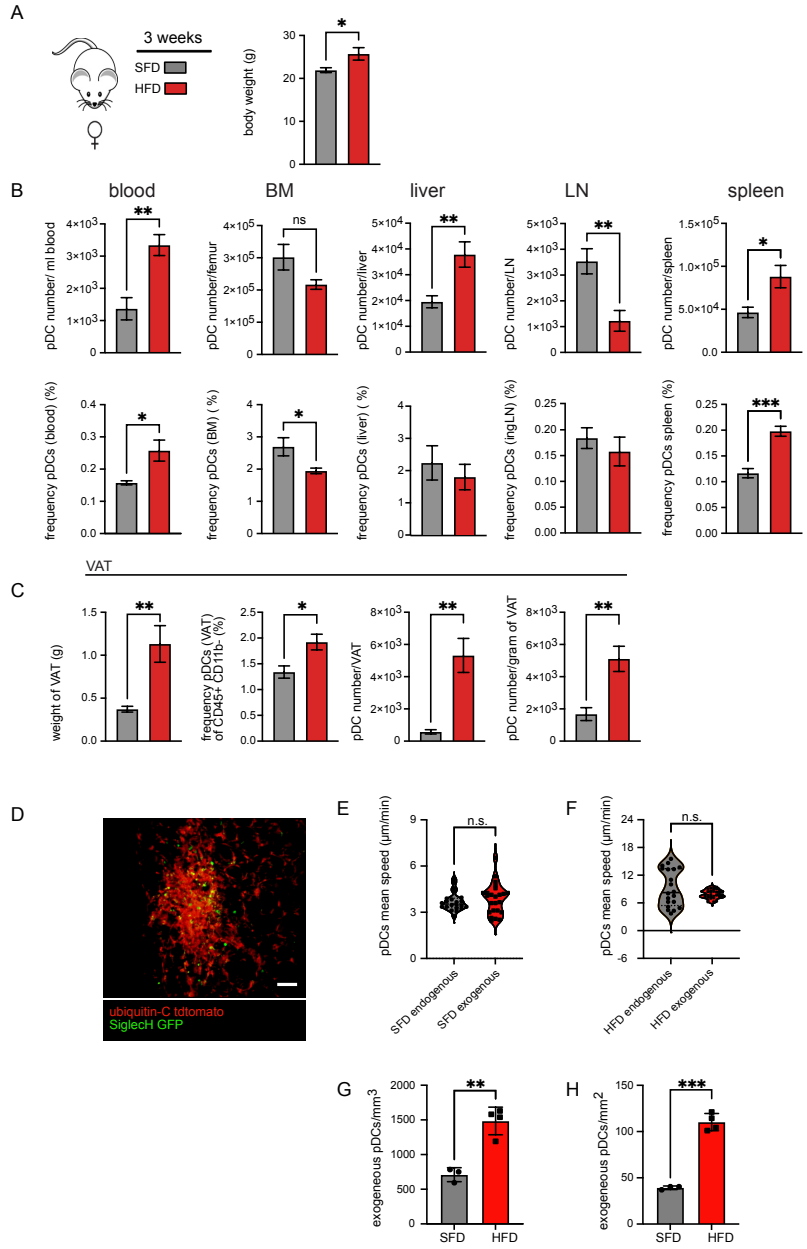


SUPPLEMENTAL FIGURE 2. **pDC location after HFD.** Female mice were fed for three weeks with SFD (black bars) or high fat diet (HFD, red bars) (A-C) and weight of body was measured (**A**). (**B**) Blood and single cell suspensions of different peripheral and lymphoid tissues of mice were analyzed by flow cytometry. BM, bone marrow; LN, inguinal lymph node. Absolute pDC numbers were calculated per 1 ml blood or per organ or femur and pDC frequency was calculated as percentage of CD45+ cells (100%). (**C**) Weight of VAT was measured and pDC frequency, total number and numbers per 1 g VAT were calculated. The animal experiment was repeated two times with 4 animals per group and similar outcome. (A-C) One representative experiment is shown. (**D**) Representative still image from multiphoton intravital microscopy of SiglecH-GFP pDCs (green) in FALC of VAT from ubiquitin-C tdtomato mice (red). Scale bar represents 70 µm. Male mice were treated for 3 weeks with SFD (**E**) or HFD (**F**) and mean migratory speed of endogenous pDCs in VAT was compared to the speed of transferred exogenous pDCs. (G-H) pDCs were enriched form SiglecH GFP mice from BM and injected i.p. After 12 h pDC distribution and numbers of these transferred pDCs were analyzed and numbers of pDCs were evaluated per volume of adipose tissue (**G**) and on the area of 3D projection images of FALCs (**H**). Statistics were performed using Student's *t*-test. Values represent mean ± SEM. *$p < 0.05$; **$p < 0.01$

**Supplemental Figure 3**

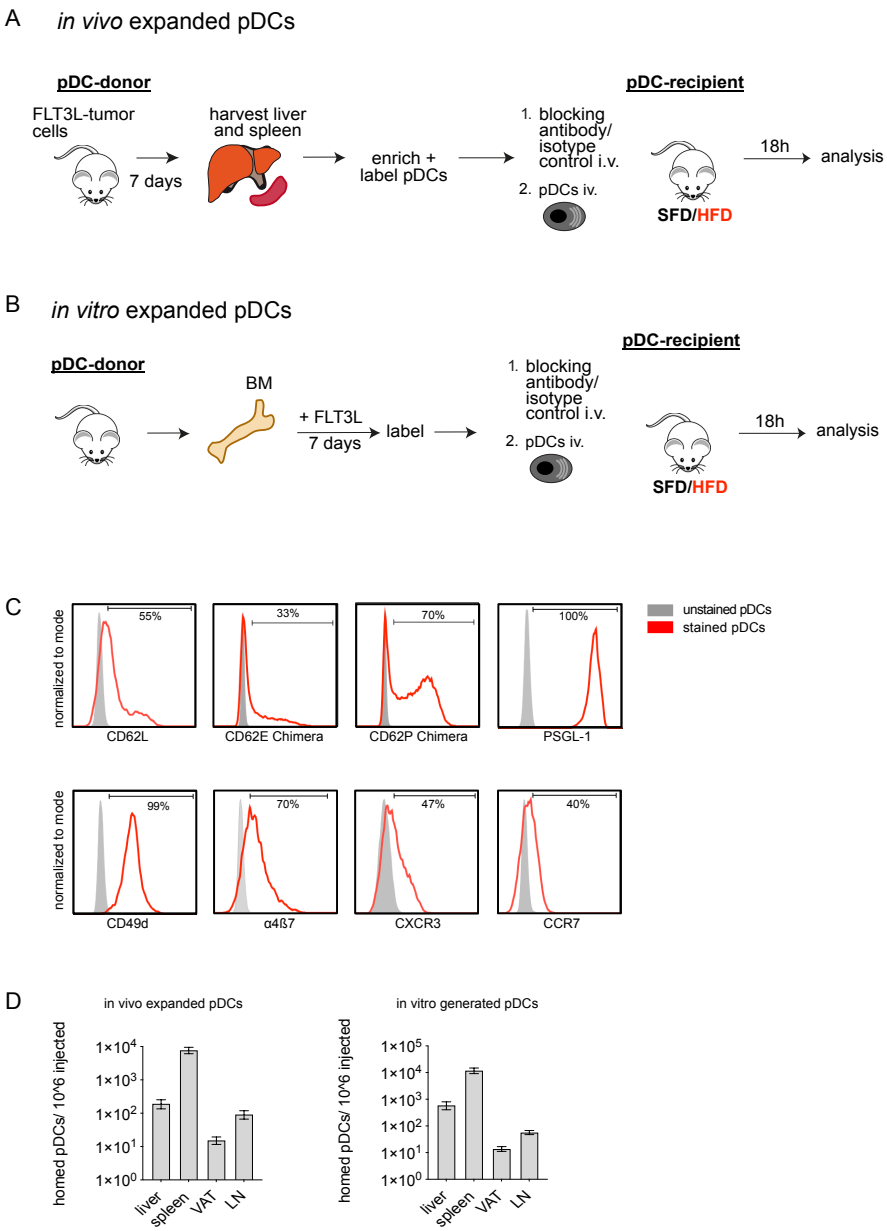


SUPPLEMENTAL FIGURE 3: **Experimental set up scheme for analyzing migration and homing profile of pDCs. (A)** Mice were implanted with B16-FLT3L secreting melanoma line for seven days and used as pDC donors. pDCs were enriched from liver and spleen, labeled and transferred into mice fed for three weeks with SFD or HFD that have been additionally treated with isotype control or blocking antibody against different epitopes. After 18 h, liver, spleen, LN and VAT were analyzed for immigrated transferred pDCs by flow cytometry. Homed pDCs were calculated per 10^6 injected pDCs. (**B**) BM was harvested from hip, femur and tibia of donor mice and cultivated for 7 days with FLT3L. Subsequently, cells were labeled and transferred into mice fed three weeks with SFD or HFD and that have been additionally treated with isotype control or blocking antibody against different epitopes. After 18 h, liver, spleen, LN and VAT were analyzed for immigrated transferred pDCs by flow cytometry. Homed pDCs were calculated per 10^6 injected pDCs. (**C**) pDC from B16-FLT3L implanted mice were enriched from liver and spleen and stained with antibodies detecting the indicated epitope (red line). Expression was compared to pDCs stained with fluorescence minus one control (FMO, grey bar). Histograms show expression pattern and frequency of pDCs expressing the indicated epitope. (**D**) Homing of *in vivo* expanded pDCs (left) and *in vitro* generated pDCs (right) 18 h after transfer into SFD treated mice.

**Supplemental Figure 4**

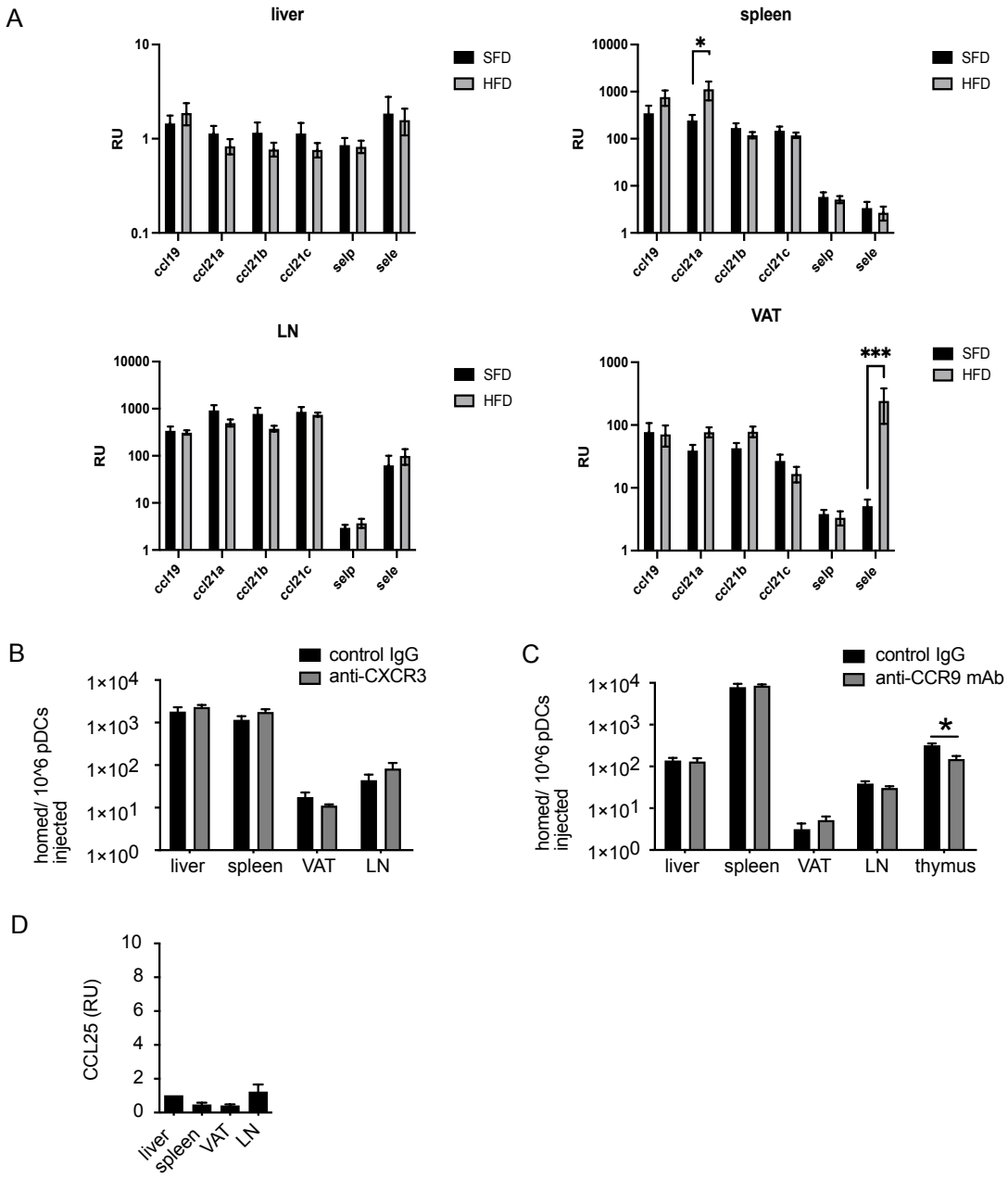


SUPPLEMENTAL FIGURE 4: **Chemokine expression and contribution for pDC homing to VAT.** (**A**) After three weeks of SFD or HFD liver, spleen, VAT and LNs were harvested and homogenized. mRNA was analyzed for relative expression of CCL19, CCL21a, CCL21b, CD62P (Selp) and CD62E (Sele) by realtime PCR and compared to 18S rRNA house-keeping gene. Liver expression levels were set as 1 and levels for spleen, VAT and LN were calculated. Relative expression units (RU) are shown in logarithmic scale. n = 3 independent experiments with 3-4 mice each. (**B**-**C**) pDCs were labeled and transferred into mice treated with isotype control or function blocking antibody against (B) CXCR3 or (C) CCR9. After 18 h, liver, spleen, LN and VAT were analyzed for immigrated pDCs by flow cytometry. (C) Additionally, thymus was analyzed for immigrated pDCs. Homed pDCs were calculated per 10^6 injected pDCs. n = 2 independent experiments with each 3-4 mice. (**D**) CCL25 expression was analyzed via Realtime-PCR and compared to 18S house-keeping gene. Liver levels were set as 1 and levels for spleen, VAT and LN were calculated. Relative expression units (RU) are shown in logarithmic scale. n = 2 independent experiments with each 3-4 mice. Statistics were performed using 2way ANOVA multiple comparison test. Values represent mean ± SEM. *$p < 0.05$, ***$p < 0.001$.

Supplemental Video Legend:

Video 1: **pDCs reside in FALC of VAT**. Uquiquitin C tdtomato mice were injected i.p. with pDCs (green, SiglecH GFP) and 18h later, VAT of male mice was imaged by multiphoton microscopy. Scale bar represents 100 µm.